Central Mediterranean tephrochronology for the time interval 250–315 ka derived from the Fucino sediment succession

NIKLAS LEICHER (iD), LORENZO MONACO, BIAGIO GIACCIO, SEBASTIEN NOMADE, ALISON PEREIRA, GIORGIO MANNELLA, SABINE WULF, GIANLUCA SOTTILI, DANILO M. PALLADINO, GIOVANNI ZANCHETTA AND BERND WAGNER (iD)

In the lacustrine succession F4-F5 of the Fucino Basin, central Italy, 20 visible tephra layers were identified in the time interval 250–315 ka (Marine Isotope Stages 8–9). Fifteen of them contained suitable material to explore their volcanic sources. Among these tephra some well-known eruptions and eruptive sequences of the Roman and Roccamonfina volcanoes were identified, such as the Tufo Giallo di Sacrofano and the Lower White Trachytic Tuff, respectively. Furthermore, the sediment succession documents a more complex eruptive history of the Sabatini, Vulsini, Colli Albani and Roccamonfina volcanic complexes during the investigated period, as inferred from previously undescribed tephra deposits. Single-crystal-fusion $^{40}Ar/^{39}Ar$ dating of two of the inspected tephra layers combined with two already published tephra ages provided the basis for a Bayesian age-depth model. The modelled tephra ages allow chronological constraining of so-far undefined eruptions of the Sabatini (272.5±4.7, 281.8±4.7, 308.5±2.8, 312.8±2.1 ka), the Vulsini (311.7±2.3, 311.9±2.3 ka) and the Colli Albani (301.0±3.6 ka) volcanic districts. Two tephra layers of an undefined volcanic source from the Roman volcanoes have modelled ages of 309.5±2.7 and 310.5±2.6 ka. The new $^{40}Ar/^{39}Ar$ and modelled ages were further used for a reassessment of the timing of already known and dated eruptive units, such as the Tufo Giallo di Sacrofano ($^{40}Ar/^{39}Ar$: 289.3±4.8 ka). Tephra tentatively correlated with the Valle Santa Maria, Case Pisello and the White Trachytic Tuff Unit E3 or Unit F offer modelled ages for these eruptions of 296.6±3.9, 301.8±3.5 and 303.6±3.4 ka, respectively. The results complete the tephrostratigraphical investigations of the c. 425 ka old F4-F5 record, extend the Mediterranean tephrostratigraphical framework and provide a significant contribution for improving knowledge on Italian volcanic explosive activity.

Niklas Leicher (n.leicher@uni-koeln.de) and Bernd Wagner, Institute of Geology and Mineralogy, University of Cologne, Zuelpicher Straße 49a, 50674 Cologne, Germany; Lorenzo Monaco, Istituto di Geologia Ambientale e Geoingegneria, CNR, Area della Ricerca di Roma 1 - Strada Provinciale 35d, 9-00010 Montelibretti, Italy; Biagio Giaccio Istituto di Geologia Ambientale e Geoingegneria, CNR, Area della Ricerca di Roma 1 - Strada Provinciale 35d, 9-00010 Montelibretti, Italy and Istituto Nazionale di Geofisica e Vulcanologia, Viadi Vigna Murata 605, 00143 Rome, Italy; Sebastien Nomade, Laboratoire des Sciences du Climat et de l'Environnement, LSCE/IPSL, UMR 8212, CEA-CNRS-UVSQ, Université Paris-Saclay, F-91190 Gif-sur-Yvette, France; Alison Pereira, Laboratoire Géosciences Paris-Saclay (GEOPS), UMR8148, Universite Paris-Saclay, F-914505 Orsay, France; Giorgio Mannella and Giovanni Zanchetta, Dipartimento di Scienze della Terra, University of Pisa, Via Santa Maria 53, 56126 Pisa, Italy; Sabine Wulf, School of the Environment, Geography and Geosciences, University of Portsmouth, Buckingham Building, Lion Terrace, Portsmouth PO3 1HE, UK; Gianluca Sottili and Danilo M. Palladino, Dipartimento di Scienze della Terra, Sapienza Universita di Roma, Piazzale Aldo Moro 5, 00185 Rome, Italy; received 15th March 2023, accepted 18th September 2023.

Tephrostratigraphy and tephrochronology are powerful tools, which find a broad range of application in archaeology, palaeoclimatology and geosciences (e.g. Lowe 2011). Due to the synchronous deposition of volcanic ash (tephra) in different sedimentary environments, tephra layers are used to set sedimentological records in a stratigraphical context and to investigate their inter-site relationships. Tephra layers also enable dating of sedimentary successions, either by radiometric dating of suitable minerals of a tephra layer or by transferring the ages of equivalent tephra layers between different sites. An outstanding advantage of tephrochronology is that chronologies developed by this method are independent of the interpretation of proxy data utilized for tuning approaches, so that, e.g. circular reasoning can be avoided and spatial and temporal evolution and relationships of different environmental systems can be assessed (Zanchetta *et al.* 2016). This is of fundamental importance, as a precise and accurate temporal framework is crucial for assessing palaeoclimatic questions and identifying short- and long-term palaeoclimatic changes and their drivers. Combining the reconstructed volcanic activity with information on palaeoenvironmental changes can also provide insights into the interactions of volcanic activity and palaeoclimate (Lavigne *et al.* 2013; Kutterolf *et al.* 2019). Moreover, tephrostratigraphy can provide valuable information for assessing volcanic hazards in terms of the frequency and magnitudes of past eruptions (Sulpizio *et al.* 2014; Albert *et al.* 2019).

However, for the successful application of tephrostratigraphy and tephrochronology allowing the transfer of reliable ages between sites, the construction of a robust tephrostratigraphical framework with extended

knowledge of the explosive volcanic history of a region and a comprehensive volcanic glass geochemical data set of the different eruptions are both needed. The Mediterranean region offers suitable conditions for tephrostratigraphy and tephrochronology, which has led to the development of a comprehensive and continuously expanding tephrostratigraphic framework (Keller *et al.* 1978; Paterne *et al.* 2008; Zanchetta *et al.* 2011; Wulf *et al.* 2012; Insinga *et al.* 2014; Petrosino *et al.* 2015; Giaccio *et al.* 2015a, 2017b; Vakhrameeva *et al.* 2018, 2021; Leicher *et al.* 2019, 2021; McGuire *et al.* 2022; Monaco *et al.* 2022b). However, the tephrostratigraphic framework >100 ka is still fragmentary.

The lacustrine succession of the Fucino Basin, central Italy (Fig. 1), has been proven to be one of the richest Mediterranean Pleistocene tephra records and greatly contributed to a more complex tephrostratigraphical framework (Giaccio *et al.* 2017b, 2019; Del Carlo *et al.* 2020; Monaco *et al.* 2021, 2022a; Leicher *et al.* 2022). Its geographical position in good range downwind of most volcanic systems of central Italy and its continuous sedimentary succession make it a corner stone to develop a reference section for volcanic activity, such as successfully shown for the last 190 ka, and provided also detailed palaeoenvironmental information (Giaccio *et al.* 2017b; Di Roberto *et al.* 2018; Mannella *et al.* 2019). The F4-F5 sediment succession obtained in 2017 from Fucino Basin extends this work for the last *c.* 425 ka (cf. Fig. 1; Giaccio *et al.* 2019) and has already greatly improved the tephrostratigraphy for the intervals 0–253 ka (Giaccio *et al.* 2019; Monaco *et al.* 2022a) and 313–425 ka (Monaco *et al.* 2021; Leicher *et al.* 2022). These results contributed towards a better knowledge of the precise timing and stratigraphical succession of Italian major volcanic eruptions, but also for preceding or following associated minor eruptive events within the Middle Pleistocene. Based on the obtained tephrochronological information, the Fucino sediment succession can be precisely dated, which is an essential prerequisite for investigating its regional palaeoenvironmental and palaeoclimatic history and allows aligning it with other Mediterranean palaeoenvironmental archives.

Here, we complement the tephrostratigraphical and tephrochronological investigations of the F4-F5 record for the pending interval 250–315 ka (marine isotope stages (MIS) 8–9), presenting new glass geochemical and chronological data of macroscopic visible tephra layers and their integration within the regional tephrostratigraphical framework.

Regional setting

Fucino Basin

The Fucino Basin is located ~650 m a.s.l. in the Abruzzo region in central Italy and is the largest extensional

tectonic basin of the central-southern Apennine chain (Fig. 1A, B). The basin opened along the E–W, NE–SW and NW–SE oriented Fucino Fault System starting from the Late Pliocene to Lower Pleistocene (e.g. Galadini & Galli 2000; D'Agostino *et al.* 2001; Giaccio *et al.* 2012; Amato *et al.* 2014). Seismic investigations of the Fucino Basin revealed a semi-graben architecture with an increasing sediment infill of up to ~900 m thickness from the west towards the depocentre in the east (Patacca *et al.* 2008). The Plio-Quaternary deposits unconformably overlay both Late Messinian terrigenous deposits and the Meso-Cenozoic carbonate basement (Cavinato *et al.* 2002; Giaccio *et al.* 2019; Mondati *et al.* 2021). The Plio-Pleistocene sedimentation is believed to have started before 2.0 Ma (Giaccio *et al.* 2015b) and 3.0 Ma (Mondati *et al.* 2021) and appears to be continuous, at least in the central part of the basin (Giaccio *et al.* 2017b, 2019; Mannella *et al.* 2019). The basin hosted Lake Fucino (Lacus Fucinus) until the lake was artificially drained, starting from the 1st–2nd century CE and completed by the end of the 19th century for agricultural reasons.

Italian volcanic activity of the Middle Pleistocene

The Pleistocene–Holocene Italian volcanism includes the volcanic activity of the Roman Province (Vulsini, Vico, Sabatini and Colli Albani volcanic districts), the Volsci Volcanic field and the Roccamonfina volcano (former Ernici-Roccamonfina Volcanic Province), the Campanian Province (Neapolitan volcanoes of Somma-Vesuvius, Campi Flegrei, Ischia and Procida and the buried Campanian Plain volcanism), Mount Vulture, the Aeolian Arc, the Sicily Province (after Peccerillo 2005; Peccerillo & Frezzotti 2015; Cardello *et al.* 2020; see also Fig. 1C). For the period investigated here (250–315 ka), explosive volcanic activity is mainly known from the Roman Province and Roccamonfina volcano and only subordinately from the Campanian Province and the Volsci Volcanic field (Fig. 1C).

In the Sabatini volcanic district (SVD), the Sacrofano caldera developed contemporaneously with the Bracciano caldera (Sottili *et al.* 2019). The age of the Tufo di Bracciano (TdB) is considered to be between 310.0±5.0, 319.1±6.0 (Sottili *et al.* 2010) and 323.9±2.0 ka (Pereira *et al.* 2017). Following the Magliano Romano Plinian fall (MRPF; 313.5±1.4 ka; Sottili *et al.* 2010; Leicher *et al.* 2022) the construction of the Monte Aguzzo Scoria cone (303.0±6.0 ka) took place, before the major caldera-forming event led to the deposition of the Tufo Giallo di Sacrofano (TGdS; 288.8±6.0 ka; Sottili *et al.* 2010). At the Bracciano caldera, the Aguscello scoria cone and Valle Santa Maria maar formed at 298.8±3.0 and 293.2±4.7 ka, respectively, prior to the creation of the Pizzo Prato caldera at 251.4±16.0 ka (Tufo di Pizzo Prato (TdPP); Sottili *et al.* 2010; Marra *et al.* 2020a). The time interval of
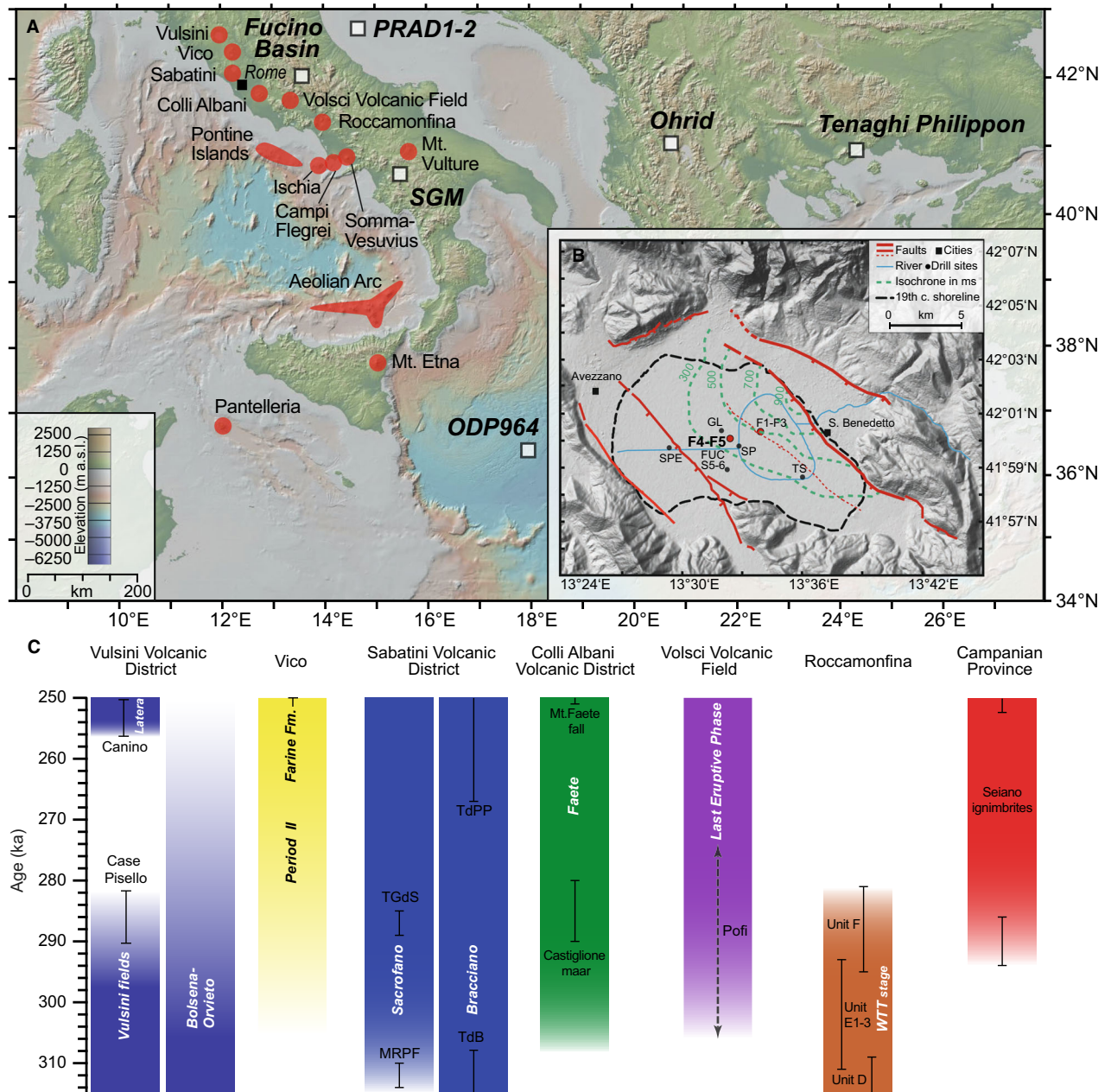
Fig. 1. A. Overview map of the central Mediterranean region and the location of Italian volcanoes (red circles) and archives discussed in the text (white squares). B. Map of the Fucino Basin and drill sites, main tectonic lines and sedimentary infill according to Cavinato *et al.* (2002). Maps made with GeoMapApp (www.geomapapp.org) based on the Global Multi-Resolution Topography by Ryan *et al.* (2009). C. Overview of the known Italian volcanic activity of the Vulsini Volcanic District (VVD), Vico volcano, Sabatini Volcanic District (SVD), Colli Albani Volcanic District (CAVD), Volsci Volcanic Field (VVF), Roccamonfina volcano and Campanian Province for the period 250–315 ka. Active periods and active volcanic complexes (coloured bars, names in italics) are presented along with the most prominent eruptions. The Aeolian Islands, Pantelleria and Mt. Vulture are not shown, since no active phases are reported in proximal settings for the period studied. TGdS = Tufo Giallo di Sacrofano; MRPF = Magliano Romano Plinian Fall; TdPP = Tufo di Pizzo Prato; TdB = Tufo di Bracciano; WTT stage = White Trachytic Tuff stage. Data source for the Vulsini volcanic district: Brocchini *et al.* (2000); Palladino *et al.* (2010); Marra *et al.* (2019); for Vico: Perini *et al.* (2004); for the Monti Sabatini volcanic district: Sottili *et al.* (2004); Sottili *et al.* (2010); for Colli Albani: Marra *et al.* (2003); Giordano *et al.* (2006); for Roccamonfina: Giannetti & Luhr (1983); Giannetti & De Casa (2000); Giannetti (2001); for the Volsci Volcanic Field: Marra *et al.* (2021); for Campanian Province: Rolandi *et al.* (2003).

interest is also characterized by various effusive activity within the SVD (Monte Rocca Romana; Monte Cinghiale; Vigna di Valle lava flows; 286–293 ka; Sottili *et al.* 2010; Marra *et al.* 2020a).

In the investigated time period, the Vico volcano activity was characterized by effusive activity of the Lago di Vico lava Formation, which led to the construction of a stratovolcano (258–305 ka; Perini *et al.* 2004), before an

explosive phase started with the Farine formation (Ignimbrite A, *c.* 250 ka; Perini *et al.* 2004).

In the Vulsini Volcanic district (VVD), only the Case Pisello eruption (293.8±4.0 ka; Brocchini *et al.* 2000) is reported as a major explosive event between the eruptions of Orvieto-Bagnoregio (WOB; 331.5±2.2 ka; Palladino *et al.* 2014; Marra *et al.* 2019; Leicher *et al.* 2022) and Canino (253.4±0.8 ka; Monaco *et al.* 2022a), although effusive and Strombolian activities were occurring in this time-span (Palladino *et al.* 2010).

In the Colli Albani Volcanic district (CAVD), the Faete Phase (De Rita *et al.* 1988), during which the Tuscolano-Artemisio peri-caldera ring fracture system and the intra-caldera Faete stratovolcano formed (Giordano *et al.* 2006, 2010), occurred at *c.* 250–308 ka (Marra *et al.* 2003) and was characterized mainly by scoria cones and lava flows, but also included the Castiglione maar succession with an estimated age of *c.* 285 ka (Marra *et al.* 2003).

The late eruptive phase of the Volsci Volcanic field (VVF) is imprecisely constrained (*c.* 230–300 ka; Marra *et al.* 2021) and is mainly characterized by effusive volcanic activity and minor local explosive activity like the Pofi cinder cone (297.6±43.3 ka; Boari *et al.* 2009b).

At the Roccamonfina volcano, a series of eruptions known as the White Trachytic Tuff (WTT) have been dated to between 230 and 330 ka (Giannetti & De Casa 2000), of which Units D (312.9±4.0 ka), E (301.5±8.0–309.9±30.0 ka) and F (292.5±14.0 ka) occurred in the investigated time frame (Giannetti & Luhr 1983; Ballini *et al.* 1991; Giannetti & De Casa 2000).

With respect to Campanian volcanoes, there is still a lack of knowledge of volcanic products older than the Campanian Ignimbrite eruption (*c.* 40 ka; Giaccio *et al.* 2017a), as those have been buried by Late Pleistocene–Holocene volcanic activity. The only accessible deposits for the investigated time interval discovered so far are the Seiano ignimbrite deposits south of the Campanian Plain, the ages of which range from *c.* 250 to 290 ka (Rolandi *et al.* 2003).

Material and methods

F4-F5 sediment record

In 2017, at the Fucino F4-F5 drill site close to the centre of the basin (Fig. 1B, latitude 42°00′06.22″N, longitude 13°32′17.79″E) two parallel core successions were recovered reaching a field depth of 87.00 and 87.75 m, respectively. Seismic information (Cavinato *et al.* 2002) and sedimentation rate estimations based on previous drilling campaigns at adjacent sites (GeoLazio and SP cores, ~20 cm ka^{-1}; Giaccio *et al.* 2015b, 2017b) suggested the F4-F5 drill site as ideal for recovering older (>190 ka) sediments at a relatively shallow depth as compared to the F1-F3 (0.45 mm a^{-1}) in the main

depocentre of the lake (Giaccio *et al.* 2017b; Mannella *et al.* 2019). Individual (1.5-m-long) core segments from both boreholes were spliced to a 98.11-m-long composite profile (F4-F5 record) based on core images, XRF data and palaeomagnetic information (Giaccio *et al.* 2019). Sediments are dominated by grey-whitish lacustrine calcareous marls alternating with darkish lacustrine clays and frequently intercalated, macroscopically visible tephra layers (*n* = 140). The variability of the calcareous content in the F4-F5 sediments is mainly related to variations in precipitation of endogenic calcite, which depends on the lake's primary productivity (Mannella *et al.* 2019). The productivity in turn is mainly controlled by temperature and hydrology, which are related to glacial–interglacial and sub-orbital climatic variability (Mannella *et al.* 2019).

The F4-F5 record spans back to MIS 12 (424.8±3.2 ka ^{40}Ar/^{39}Ar age of TF-85; Giaccio *et al.* 2019), significantly extending the previous F1-F3 record (last 190 ka; Giaccio *et al.* 2017b, 2019; Mannella *et al.* 2019), and has already been subject to a series of detailed tephrostratigraphical and tephrochronological investigations focusing on specific intervals: 170–253 ka (Monaco *et al.* 2022a), 313–366 ka (Leicher *et al.* 2022), 365–424 ka (Monaco *et al.* 2021). Here, the remaining interval 250–315 ka is investigated.

X-ray fluorescence (XRF) core scanning

Individual core halves of the F4-F5 record were scanned using an Itrax XRF scanner (Cox Analytical Systems, Sweden) at the Institute of Geology and Mineralogy of the University of Cologne, Germany. XRF scans were made as described in Giaccio *et al.* (2019) using a Chromium tube set at 55 kV and 30 mA with a dwell time of 10 s and a step-size of 2.5 mm.

Tephra identification and sample preparation

Tephra layers in the F4-F5 Fucino record were identified during visual core description and subsequent inspection of high-resolution line-scan images. Tephra layers were sampled over their entire thickness as a bulk sample and, if different subunits were identified, a subsample was taken from each subunit (Table 1). If tephra layers of thickness <0.5 cm were mixed with substantial amounts of lake sediments, samples were sieved and treated with HCl (10%, room temperature <12 h) to remove carbonates and enrich the glass fraction.

Sampling of the proximal Tufo Giallo di Sacrofano (TGdS) deposits

The TGdS was sampled at two sites at the northern rim of the Sacrofano caldera of the Sabatini Volcanic District. At site A (42°8′34.00″N, 12°23′45.00″E), TGdS deposits are separated by a palaeosol from underlying local scoria

Table 1. Tephra layers identified in the time interval 250–315 ka of the F4-F5 succession and information about their position within the record, appearance, petrological composition according to the TAS-diagram (Le Bas *et al.* 1986) and their modelled and $^{40}Ar/^{39}Ar$ ages. † = $^{40}Ar/^{39}Ar$ ages of this study; ‡ = $^{40}Ar/^{39}Ar$ age from Monaco *et al.* (2022a); ‡‡ = $^{40}Ar/^{39}Ar$ age from Leicher *et al.* (2022). Tephra layers written in italics represent altered material.

Label	Core section and depth (cm)	Bottom depth (m c.d.)	Distance to tephra above (m)	Thickness (cm)	Appearance	Rock type (TAS)	Modelled age and $^{40}Ar/^{39}Ar$ age (ka)
TF-43	F4-32 149.80–151.21	49.021	0.47	1.96	Layer	Phonolite-trachyte	253.9±1.5, 253.4±0.8‡
TF-44	*F4-33 48.00–51.00*	*49.542*	*0.52*	*3.00*	*Lenses*	*Altered*	*257.9±3.1*
TF-45	*F4-33 128.50–130.00*	*50.332*	*0.79*	*1.50*	*Lenses*	*Altered*	*263.9±4.3*
TF-46	F5-34 31.00–32.00	51.453	1.12	5.97	Lenses	Tephrite-phonotephrite	272.5±4.9
TF-47	F4-35 26.00–31.97	52.681	1.23	2.86	Lenses	Trachyandesite-phonolite-trachyte	281.8±4.7
TF-48	F5-35 85.49–88.35	53.899	1.22	1.00	Layer	Trachyandesite-phonolite-trachyte	287.8±4.2, 289.3±4.8†
TF-49	*F5-35 120.26–123.45*	*54.250*	*0.35*	*3.19*	*Layer*	*Altered*	*289.2±4.2*
TF-50	*F5-36 74.00–78.25*	*55.660*	*1.41*	*4.25*	*Lenses*	*Altered*	*294.5±4.1*
TF-51	F5-36 130.75–133.5	56.212	0.55	2.75	Lenses	Phonotephrite	296.6±3.9
TF-52	*F5-36 148.89–149.31*	*56.370*	*0.16*	*0.42*	*Layer*	*Altered*	*297.2±3.9*
TF-53	F5-37 70.14–71.93	57.385	1.01	1.79	Layer	Foidite-tephriphonolite	301.0±3.6
TF-54	F5-37 89.99–91.63	57.582	0.20	1.64	Layer	Tephriphonolite-phonotephrite + phonolite	301.8±3.5
TF-55	F5-37 138.38–139.28	58.058	0.48	0.90	Layer	Phonolite-trachyte	303.6±3.4
TF-56	F5-38 107.25–110.25	59.363	1.31	3.00	Layer	Phonotephrite-tephriphonolite + phonolite	308.5±2.8
TF-57	F5-38 136.90–137.36	59.634	0.27	0.46	Layer	Tephrite-phonotephrite-tephriphonolite	309.5±2.7
TF-58	F4-39 17.99–25.00	59.886	0.25	8.00	Layer	Tephrite-phonotephrite-tephriphonolite-phonolite	310.5±2.6
TF-59	F4-39 55.00–58.00	60.216	0.33	3.00	Layer + lenses	Phonotephrite-tephriphonolite-trachyandesite	311.7±2.3
TF-60	F4-39 60.00–62.00	60.256	0.04	2.00	Lenses	Phonotephrite-tephriphonolite-trachyandesite	311.9±2.3
TF-61 top/bottom	F4-39 79.75–81.5–84.75	60.483	0.23	5.00	Twofold zoned layer	Top = phonotephrite-tephriphonolite, bottom = tephrite	312.8±2.1, 313.3±1.0†
TF-62 top/middle/bottom	F4-39 90.00–94.20–97.60–100.50	60.608	0.12	10.50	Threefold zoned layer	Top = phonolite + tephriphonolite, middle = phonolite + tephriphonolite, bottom = phonolite + tephrite-phonotephrite	313.2±2.2, 313.5±1.4‡‡

cone deposits and sample TGDS-1 was taken from the basal part of the TGdS deposits represented by ~1–2 m thick blackish, well-sorted, cm-sized scoria of the initial phase of the eruption. TGDS-2 is a sample from the overlying basal part of the main eruptive phase represented by yellowish, partly zeolitized ash deposits of several-m-thickness. At site B (42°8′5.00″N, 12°23′45.00″E), only the TGdS products of the main phase are exposed on top of Monte Ficoreto scoria cone deposits. Samples TGDS 3–4 were sampled from the middle and the bottom, respectively, of this >10-m-thick succession.

EPMA-WDS

Major and minor elements of individual glass fragments were analysed by electron microprobe wavelength dispersive spectroscopy (EPMA-WDS) to determine the geochemical fingerprint of the respective tephra layers of the Fucio succession and proximal TGdS samples. All samples were measured at the University of Cologne (Germany), whereas one sample (TF-47) was also measured at the Istituto di Geologia Ambientale e Geoingegneria of the Italian National Research Council (IGAG-CNR, Rome, Italy). A JEOL JXA-8900RL electron microprobe equipped with five wavelength dispersive spectrometers was used for analysis at the University of Cologne. The operation conditions were set to 12-kV accelerating voltage, 6-nA beam current and 5–10 μm beam diameter. Full details of calibration and measuring conditions are given in Leicher (2021). Analysis at IGAG-CNR were performed with a Cameca SX50 electron microprobe equipped with five wavelength dispersive spectrometers and operated with an accelerating voltage of 15 kV, a beam current of 15 nA, a beam diameter of 10 μm and a counting time of 20 s per element (full details of calibration and measuring conditions are given in Leicher & Giaccio (2021)). Analytical differences caused by the different EPMA-WDS settings of the IGAG-CNR and University of

Cologne laboratories are discussed in detail in Leicher *et al*. (2021). This previous comparison revealed higher results for SiO_2 and MgO and lower for FeO, Mn, Na_2O of the IGAG-CNR analyses relative to those obtained at the University of Cologne, whereas concentrations of TiO_2, Al_2O_3, CaO and Cl do not show systematic deviations. With respect to sample TF-47, results of both laboratories fully overlap within the compositional spectrum of the sample, and so no correction was applied. However, as observed within the previous comparison, IGAG-CNR results trend towards the overall upper range of SiO_2 and lower range of Na_2O concentrations measured for TF-47.

During microprobe analysis at the University of Cologne, MPI-DING glasses (ATHO-G; StHs6/80-G) were used as secondary standards to evaluate the accuracy and precision of measurement sessions based on preferred values from Jochum (2006). Mean values for precision (relative standard deviation %) and accuracy (bias of mean to preferred reference value in %) of analyses are respectively up to 1.4 and 1.1% for elemental concentrations >60 wt%, up to 3.2 and 2.6% for 25–5 wt %, up to 8.2 and 9.2% for 5–1 wt%, up to 11.3 and 10.0% for 1–0.2 wt% and 61 and >18% for 0.2–0.1 wt%.

The EPMA laboratory at IGAG-CNR used the Kakanui augite USNM 122142 (Jarosewich 2002) and rhyolite RLS132 glass from the United States Geological Survey (Huebner & Woodruff 1985) as secondary reference material prior to sample measurements to evaluate data quality. The mean analytical precision and accuracy are respectively up to 1.8 and 0.2% for element abundances >50 wt%, up to 2.7 and 3.8% for element abundances between 20–10 wt%, up to 5.8 and 9.5% for element abundances between 9–4 wt%, up to 3.0 and 5.3% for element abundances 2–1 wt%, up to 40.8 and 18.1% for element abundances 1.0–0.1 wt% and up to 23.3 and 54.4% for element abundances <0.1 wt%.

Only EPMA-WDS geochemical analyses of glass fragments with analytical totals >90 wt% were considered and normalized to 100% on a water-free basis, excluding volatiles (Cl, SO_3 and F). The tephra layers were classified according to their geochemical glass composition using the total alkali vs. silica (TAS) classification system (Le Bas *et al*. 1986).

$^{40}Ar/^{39}Ar$ dating

Two tephra layers (TF-48/-61, see Table 1 for depths) were selected for dating and subsequently sieved using mesh sizes of 500, 350 and 250 μm. For tephra TF-48, the 500–350 and 350–250 μm fractions were further separated using a FRANTZ magnetic separator at the University of Cologne. All aliquots were washed with distilled water before transparent, inclusion-free sanidine and/or leucite crystals were handpicked under a binocular and sent to the Laboratoire des Sciences du Climat et de l'Environnement (CEA, CNRS UMR 8212, Gif-sur-

Yvette, France). At CEA, crystal aliquots underwent an additional purity screening and were selected based on available crystal sizes for irradiation and dating (500–350 μm fraction for TF-61 and 350–250 μm fraction for TF-48). Between 20 and 30 crystals for each tephra layer were irradiated at the CLICIT facility of the Oregon State University TRIGA reactor before individual minerals were measured by means of single crystal $^{40}Ar/^{39}Ar$ fusion at the CEA. Neutron fluence *J* factor was calculated using co-irradiated Alder Creek sanidine standard ACs-2 associated with an age of 1.1891 Ma (Niespolo *et al*. 2017) according to the K total decay constant of Renne *et al*. (2011) ($\lambda_{e.c.} = (0.5757\pm0.016)\times10^{-10}$ a^{-1} and $\lambda_{\beta}^{-} = (4.9548\pm0.013)\times10^{-10}$ a^{-1}). *J*-values are the following: TF-48 ($J = 0.00055581\pm0.00000139$; TF-61 ($J = 0.0005606\pm0.00000045$). A detailed description of analytical settings can be found in Leicher *et al*. (2022) and full analytical data for each sample can be found in Table S1.

Age-depth modelling

Age-depth modelling for the studied interval of the F4-F5 succession was performed using the software package Bacon v. 2.5.8 (Blaauw & Christen 2011) within the open-source statistical environment R (R Core Team 2022) and used four available $^{40}Ar/^{39}Ar$ ages of tephra layers identified within the sediment succession. The entire succession was divided into 5-cm vertical sections to model individual accumulation rates at a 99% confidence interval, which provide the basis for the age-depth model. Major sedimentological changes identified during core description and within the XRF-downcore data were considered via the 'boundary' function within the model to account for different sedimentation rates during glacial and interglacial conditions. This major lithological change (carbonate and clastic content) was identified at about 53.1 m correlated depth (m c.d.) and marks the change from interglacial (MIS 9) to glacial (MIS 8) conditions (Giaccio *et al*. 2019; Mannella *et al*. 2019). Based on the age-depth model, an individual age with a 2σ uncertainty was calculated for each tephra layer identified.

Results

$^{40}Ar/^{39}Ar$ dating results and age-depth modelling

The results of $^{40}Ar/^{39}Ar$ dating of individual tephra layers are presented as probability diagrams (Fig. 2). Weighted mean age uncertainties are reported at 2σ, including *J* uncertainty, and were calculated using Isoplot 4.1 (Ludwig 2009). Inverse isochrones of individual samples, although imprecise for tephra TF-48, are characterized within uncertainties by an atmospheric $^{40}Ar/^{36}Ar$ initial intercept, suggesting that dated crystals are without detectable excess argon. The full inverse

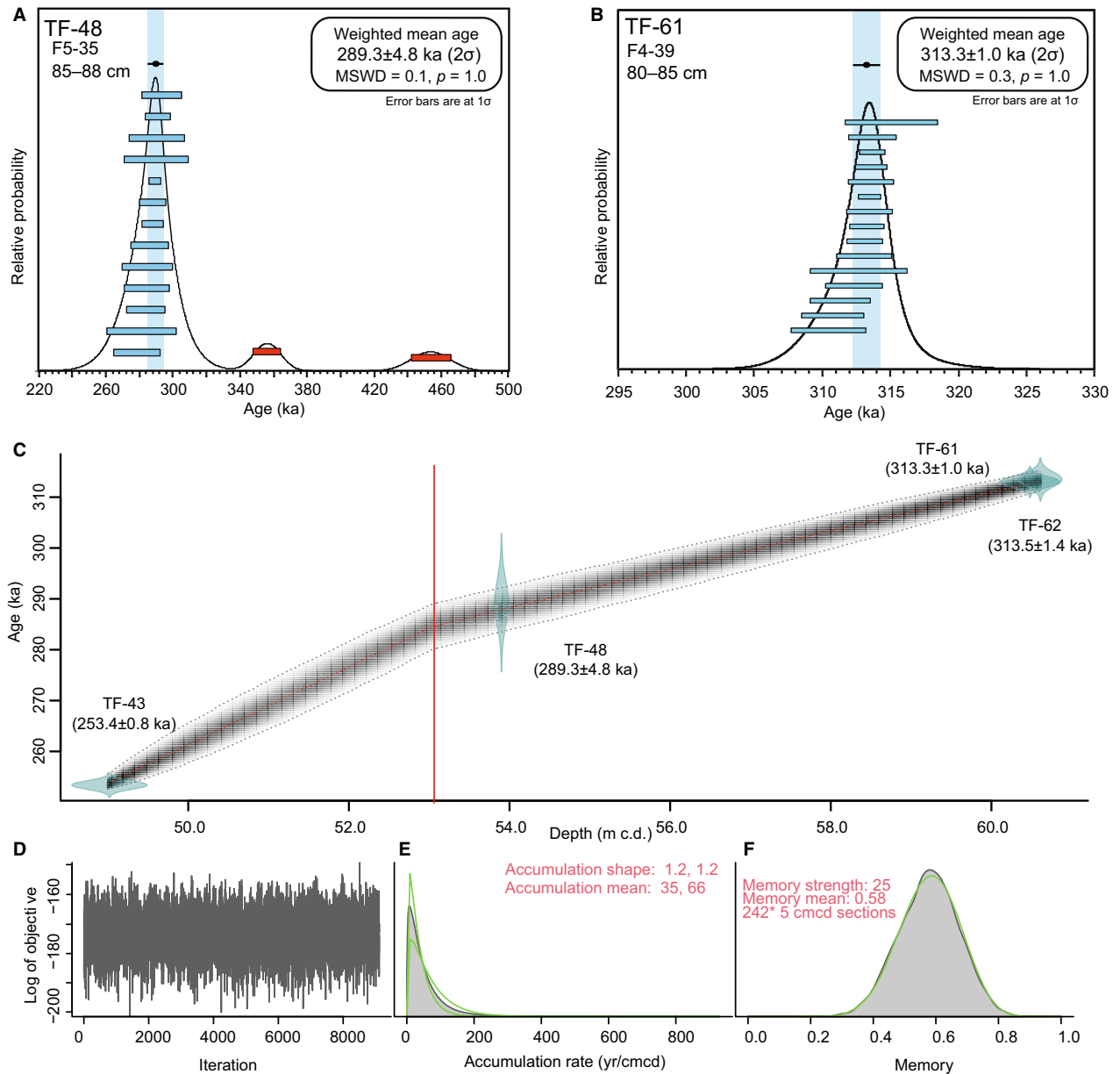*Fig. 2.* A, B. Relative probability diagrams of single crystal fusion ^{40}Ar/^{39}Ar ages of tephra layers TF-48 and TF-61. C–F. Age-depth model (C) based on available ^{40}Ar/^{39}Ar ages of tephra layers of the studied interval, modelled using Bacon v. 2.5.8 (Blaauw & Christen 2011). The red line indicates the position of the boundary function, which was set within the model to account for differences in the accumulation rate during glacial and interglacial conditions. D. Graph showing the fit of all Markov Chain Monte Carlo iterations of the model run. E, F. Prior (green) and posterior (grey) distributions of accumulation rate (E) and memory (F) for the modelled succession of F4-F5 along with the chosen input parameter.

isochrones data set can be found in Table S1. A total of 15 individual sanidine and leucite crystals of TF-48 were dated. The main population, constituted by 13 crystals (Fig. 2), was used to calculate a weighted mean age of 289.3±4.8 ka (MSWD = 0.1, *p* = 1.0). Two older crystals were also found (356.0±16.4, 454.0±23.4 ka). The age of tephra layer TF-61 was determined based on 15 leucite single crystals, which share within uncertainties the same age (Fig. 2). This allowed the calculation of a robust and precise weighted mean age of 313.3±1.0 ka (MSWD = 0.3, *p* = 1.0).

The two new ^{40}Ar/^{39}Ar ages and the previously obtained ages for TF-62 (313.5±1.4 ka; Leicher *et al.* 2022) and TF-43 (253.4±0.8 ka; Monaco *et al.* 2022a) provided the basis for age-depth modelling of the studied interval (Fig. 2). Overall, the model suggests continuous sedimentation with a mean accumulation rate of 67.6 a cm^{-1} (14.8 cm ka^{-1}) during glacials and 41.1 a cm^{-1} (24.3 cm ka^{-1}) during interglacial conditions. The modelled ages of the tephra layers that have not been directly dated are provided in Table 1. All ^{40}Ar/^{39}Ar ages of tephra layers discussed from literature were

recalculated according to ACs at 1.1891 Ma (Niespolo *et al.* 2017) and the total K decay constant of Renne *et al.* (2011) and are summarized in Table 2.

Tephra identification, morphological description and compositional features

Within the interval 49.00–60.61 m c.d. of the F4-F5 sediment succession 20 layers containing pyroclastic material were identified by visual inspection. The position of these tephra horizons and their characteristic lithological features, i.e. thickness, colour, morphological appearance, are given in Table 1. Often, tephra occurs as massive discrete layers or single or arrays of lenses intercalated in fine grained lake sediments and vary in thickness between 0.4 and 10.5 cm. Bioturbation, sediment load, or drilling disturbance structures are present, but had a minor effect on the preservation of most of the tephra layers with respect to determining the position of the isochrone or internal structures. Tephra layers TF-43 and TF-62,

framing the here investigated interval, were previously analysed and correlated with the Canino eruption from the VVD (Monaco *et al.* 2022a) and the Magliano Romano Plinian Fall (MRPF) eruption of the SVD (Leicher *et al.* 2022), respectively. Of the remaining 18 tephra layers, 13 contained sufficient amounts of fresh glass for detailed geochemical fingerprinting. The other five tephra layers, in which glass was absent or affected by devitrification processes, are found in the interval 49.02–56.37 m c.d. This partially extends the interval from ~46–49 m c.d., in which methane–sediment interactions have caused alteration of volcanic glass as described by Monaco *et al.* (2022a). However, similar to the interval described before, not all tephra layers were affected by alteration. The full data set of EPMA-WDS analyses is available at the EarthChem repository (Leicher *et al.* 2023). The individual petrological classification of tephra layers according to the total alkali vs. silica (TAS) diagram (Le Bas *et al.* 1986) is summarized in Table 1 and visualized in Fig. 3.

Table 2. Summary of available ^{40}Ar/^{39}Ar ages discussed in the text and in Fig. 8. For a homogenized comparison, all ages were recalculated to ACs at 1.1891 Ma (Niespolo *et al.* 2017) and the decay constant of Renne *et al.* (2011). Uncertainties are given at a 2σ level including analytical and J-value uncertainties. N/A = no information about decay constant and mineral flux standards in original reference available for recalculation.

| Volcanic source	Eruptive event/name of tephra	Original age (ka)	Recalculated age (ka)	Reference
Campanian	Seiano (VE-2A)	245.9±3.0	250.3±6.0	Rolandi *et al.* (2003)
Campanian	Seiano (VE-2B)	289.6±3.8	294.8±3.8	Rolandi *et al.* (2003)
Campanian	Val D'Agri Tephra	265.1±6.0	264.2±6.0	D'Addezio *et al.* (2006)
RMF	WTT Unit F	288.0±14.0	292.5±14.0	Giannetti & De Casa (2000)
RMF	LWTT Unit E 3	297.0±8.0	301.5±8.0	Giannetti & De Casa (2000)
RMF	LWTT Unit E 3	307.0±4.0	N/A	Giannetti & Luhr (1983)
RMF	LWTT Unit E 3	295.0±2.0	N/A	Ballini *et al.* (1991)
RMF	LWTT Unit E 1	301.0±2.0	N/A	Ballini *et al.* (1991)
RMF	LWTT Unit E 1	305.0±30.0	309.9±30.0	Giannetti & De Casa (2000)
RMF	LWTT Unit D	308.0±4.0	312.9±4.0	Giannetti & De Casa (2000)
RMF	LWTT Unit E1 (MOL10/14)	311.0±5.0	312.1±5.0	Amato *et al.* (2014)
SVD	Pizzo di Prato (SVD-01)	249.0±16.0	251.4±16.0	Sottili *et al.* (2010)
SVD	Vigna di Valle lava (SAB-14)	283.0±6.0	285.8±6.0	Sottili *et al.* (2010)
SVD	TGDS (R93-28)	285.0±2.0	289.7±2.0	Karner & Renne (1998)
SVD	TGDS (SAB-49)	286.0±6.0	288.8±6.0	Sottili *et al.* (2010)
VVD	Case Pisello	286.0±8.0	293.8±4.0	Brocchini *et al.* (2000)
SVD	M. Rocca Romana (MRR)	288.1±5.9	288.8±5.9	Marra *et al.* (2020a)
SVD	M. Cinghiale lava (MCG)	292.7±1.8	293.4±1.8	Marra *et al.* (2020a)
SVD	Valle Santa Maria (VSM)	292.7±4.7	293.2±4.7	Marra *et al.* (2020a)
SVD	Aguscello (SAB-19)	296.0±3.0	298.9±3.0	Sottili *et al.* (2010)
SVD	M. Aguzzo Scoria cone (SAB-50)	300.0±6.0	303.0±6.0	Sottili *et al.* (2010)
SVD	Tufo di Bracciano (SAB-15)	307.0±5.0	310.0±5.0	Sottili *et al.* (2010)
SVD	Tufo di Bracciano (SAB-71)	316.0±6.0	319.1±6.0	Sottili *et al.* (2010)
SVD	Tufo di Bracciano (POL12-01/03)	325.0±2.0	323.9±2.0	Pereira *et al.* (2017)
VVD	CB-5	313.3±6.9	313.6±6.9	Marra *et al.* (2020b)
VVD	CB-4	313.5±22.1	313.8±22.1	Marra *et al.* (2020b)
VVD	CB-5	315.3±6.9	315.6±6.9	Marra *et al.* (2020b)
Undefined	PdG-S13	248.1±3.9	247.3±3.9	Marra *et al.* (2016)
Undefined	R93-15H2	253.0±8.0	252.2±8.0	Marra *et al.* (2016)
Undefined	PdG-S22	262.9±5.0	262.0±5.0	Marra *et al.* (2016)
Undefined	PdG-S23	265.0±8.0	264.1±8.0	Marra *et al.* (2016)
Undefined	PdG-S4+R95-04B	269.2±3.8	268.3±3.8	Marra *et al.* (2016)
Undefined	AV-AF	277.9±1.6	277.0±1.6	Marra *et al.* (2016)
Undefined	PdG-S19	297.3±2.2	297.3±2.2	Marra *et al.* (2016)
Undefined	Casal de' Pazzi (CdP)	303.5±9.0	302.5±9.0	Marra *et al.* (2018)
Undefined	KW-1	309.5±4.3	310.2±4.3	Marra *et al.* (2023)
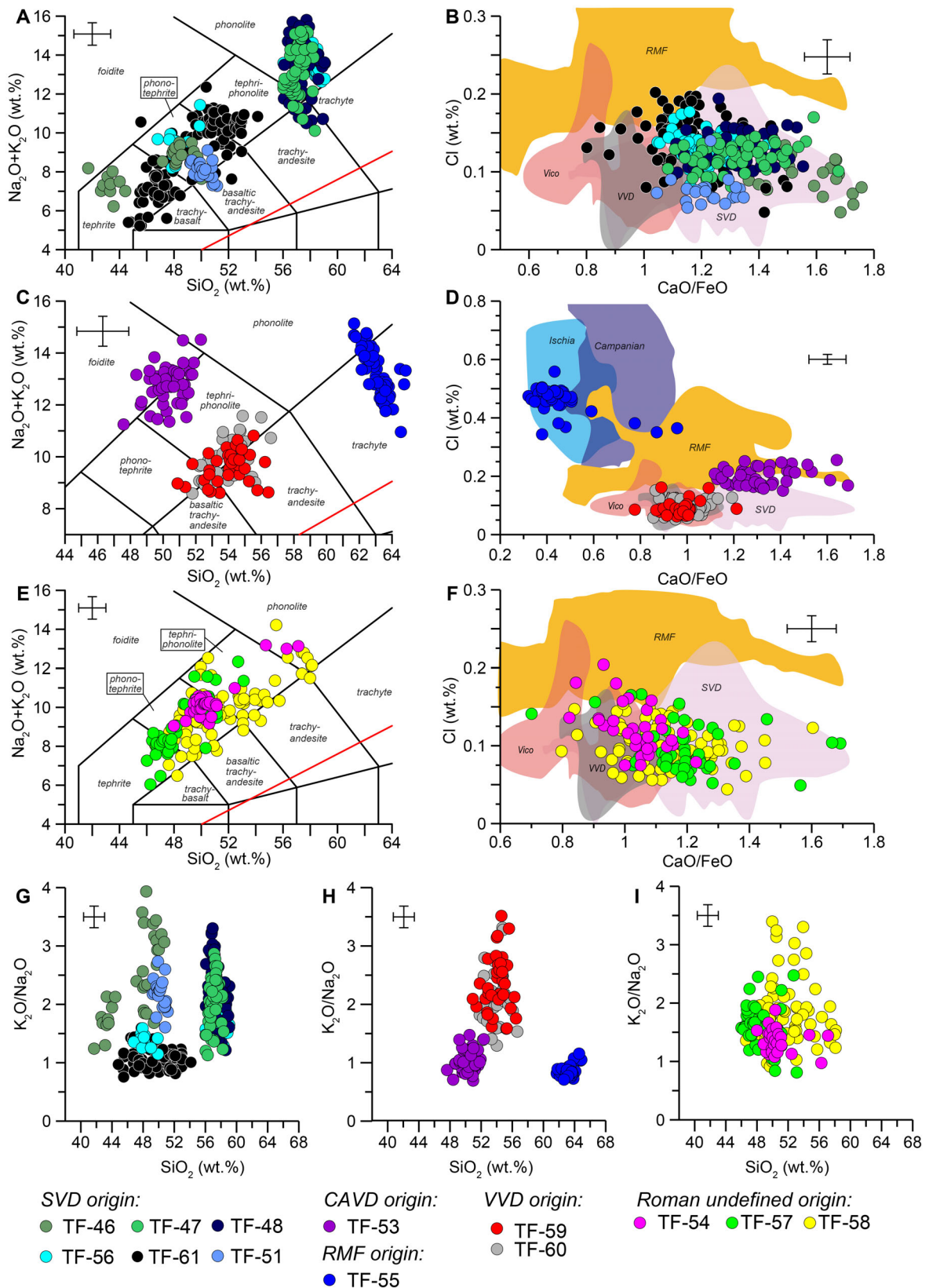
Fig. 3. Geochemical classification and overview of F4-F5 tephra layers investigated. A, C, E: TAS classification according to (Le Bas *et al.*, 1986). B, D, F: CaO/FeO vs. Cl diagrams show the different volcanic origins based on Giaccio *et al.* (2017b). G, H, I: SiO$_2$ vs. K$_2$O/Na$_2$O diagrams of the respective tephra layers. Error bars represent the twofold standard deviation of replicate analyses of ATHO-G.

Volcanic sources of tephra layers

General compositional features of investigated tephra layers

Tephra layers show the entire suite of rocks known from peri-Tyrrhenian volcanoes, but are dominated by tephritic to phonolitic compositions (*n* = 17). Only one tephra had a phonolitic-trachytic composition. Based on their compositional differences and positions within the CaO/FeO vs. Cl diagram, the tephra layers are discussed according to their proposed volcanic source. The majority of compositions suggest an origin from the Roman volcanoes (Sabatini Volcanic District (SVD), Vulsini Volcanic District (VVD), Colli Albani Volcanic District (CAVD)), but there is also evidence of activity from the Roccamonfina volcano (RMF) (Fig. 3).

Sabatini volcanic district (SVD) tephra

TF-46 (modelled age 272.5±4.9 ka). – The composition of TF-46 reveals a tephritic and a phonotephritic compositional group, with no intermediate compositions in the SiO$_2$ range between 44.4 and 47.2 wt%. Mean alkali ratios of tephrites are 1.7, whereas phonotephrites are at 2.8. Both groups plot within the CaO/FeO vs. Cl diagram in the field of the SVD. Major explosive activity of the SVD in that time range is reported from the Pizzo Prato (251.4±16.0 ka; Sottili *et al.* 2010) and Tufo Giallo di Sacrofano (TGdS, 288.8±6.0 ka; Sottili *et al.* 2010) eruptions, but chronological and compositional variations preclude a firm correlation of TF-46 with either eruption (Fig. 4G–J). Interestingly, the less evolved part of the initial phase of the TGdS eruption (TGDS-1) does show a general similarity with TF-46 (Fig. 4), suggesting that TF-46 may represent a so far undescribed eruption of the SVD. A tephra layer found in the Val d'Agri in the Southern Apennines was dated at a very similar age of 264.2±6.0 ka, but was related to the ancient Seiano ignimbrites of the Neapolitan volcanoes (D'Addezio *et al.* 2006).

TF-47/-48 (TF-47 modelled age 281.8±4.7 ka, TF-48 $^{40}Ar/^{39}Ar$ age 289.3±4.8 ka). – TF-47 and TF-48 both have a phonolitic to trachytic composition with high alkali ratios (mean K$_2$O/Na$_2$O = 2.0). Along with their position in the CaO/FeO vs. Cl diagram an origin from the SVD is suggested. TF-48 has been $^{40}Ar/^{39}Ar$ dated at 289.3±4.8 ka, which is in good accordance with the age of 288.8±6.0 ka of the TGdS eruption of the SVD (Sottili *et al.* 2010). Both Fucino tephra overlap in their composition with the main eruptive phase of the TGdS (TGdS-2–4), but show a wider range of CaO, FeO, TiO$_2$, MgO values (Fig. 4). However, based on the good chronological match a correlation of TF-48 and the TGdS is most likely. A correlation of TF-47 with the Pizzo Prato eruption, known as the next younger major

eruptive event of the SVD, can be ruled out, as geochemical compositions (Monaco *et al.* 2022a) and their ages differ, even though the current age of the Pizzo Prato eruption is imprecise (251.4±16.0 ka; Sottili *et al.* 2010). Tephra TF-47 also differs from a tephra originating from the SVD, which was found in the sediment successions from Lake Ohrid (270.6±4.9 ka; OH-DP-1175, PE-0294.8; Leicher *et al.* 2022; Wagner *et al.* 2023) and can now be identified as a distal Pizzo Prato equivalent based on the geochemical data from Monaco *et al.* (2022a). Since TF-47 differs from the general more silica undersaturated, foiditic composition of the CAVD (Marra *et al.* 2003; Boari *et al.* 2009a), the Castiglione maar succession (*c.* 285 ka; Marra *et al.* 2003) is excluded as potential equivalent deposit and TF-47 is interpreted to represent an unknown eruption from the SVD.

TF-51 (modelled age 296.6±3.9 ka). – TF-51 has a phonotephritic composition (with a relatively high mean alkali ratio of 2.2 and plots mainly within the field of the SVD within the CaO/FeO vs. Cl diagram (Fig. 3B). The composition of TF-51 is similar to that of older SVD products (TF-61, MRPF; Fig. 5C–H) from which several minor eruptive events of similar age have been reported. A phreatomagmatic surge of the Valle Santa Maria crater was dated at 293.2±4.7 ka (Marra *et al.* 2020a) and the Monte Aguzzo Scoria cone at 303.0±6.0 ka, but no glass geochemical analyses have yet been conducted for either of these.

TF-56 (modelled age 308.5±2.8 ka). – Tephra TF-56 has a twofold composition with a phonotephritic to tephriphonolitic and a phonolitic part with mean alkali ratios of 1.4 and 1.8, respectively. The position in the CaO/FeO vs. Cl diagram suggests an origin from the SVD. The geochemical composition of TF-56 is similar to tephra TF-62 (Fig. 5C–H), which is correlated with the Magliano Romano Plinian Fall (MRPF) eruption of the SVD (313.5±1.4 ka; Leicher *et al.* 2022). However, eruptive events of the Sacrofano caldera following directly the MRPF have not yet been reported in proximal settings (Sottili *et al.* 2010; Marra *et al.* 2020a). From the Bracciano caldera, the age for the Tufo di Bracciano eruption is constrained between 310.0±5.0 ka (Sottili *et al.* 2010) and 323.9±2.0 ka (Pereira *et al.* 2017), but has not been investigated for its geochemical composition. Therefore, the correlation of TF-56 with a specific eruption of the SVD is still pending at this point.

TF-61 ($^{40}Ar/^{39}Ar$ age 313.3±1.0 ka). – TF-61 has a lithological zonation with a blackish bottom unit of tephritic glass composition and a greyish top unit dominated by a phonotephritic to tephriphonolitic composition. The majority of analyses of both units show a dominating SVD-like composition with few
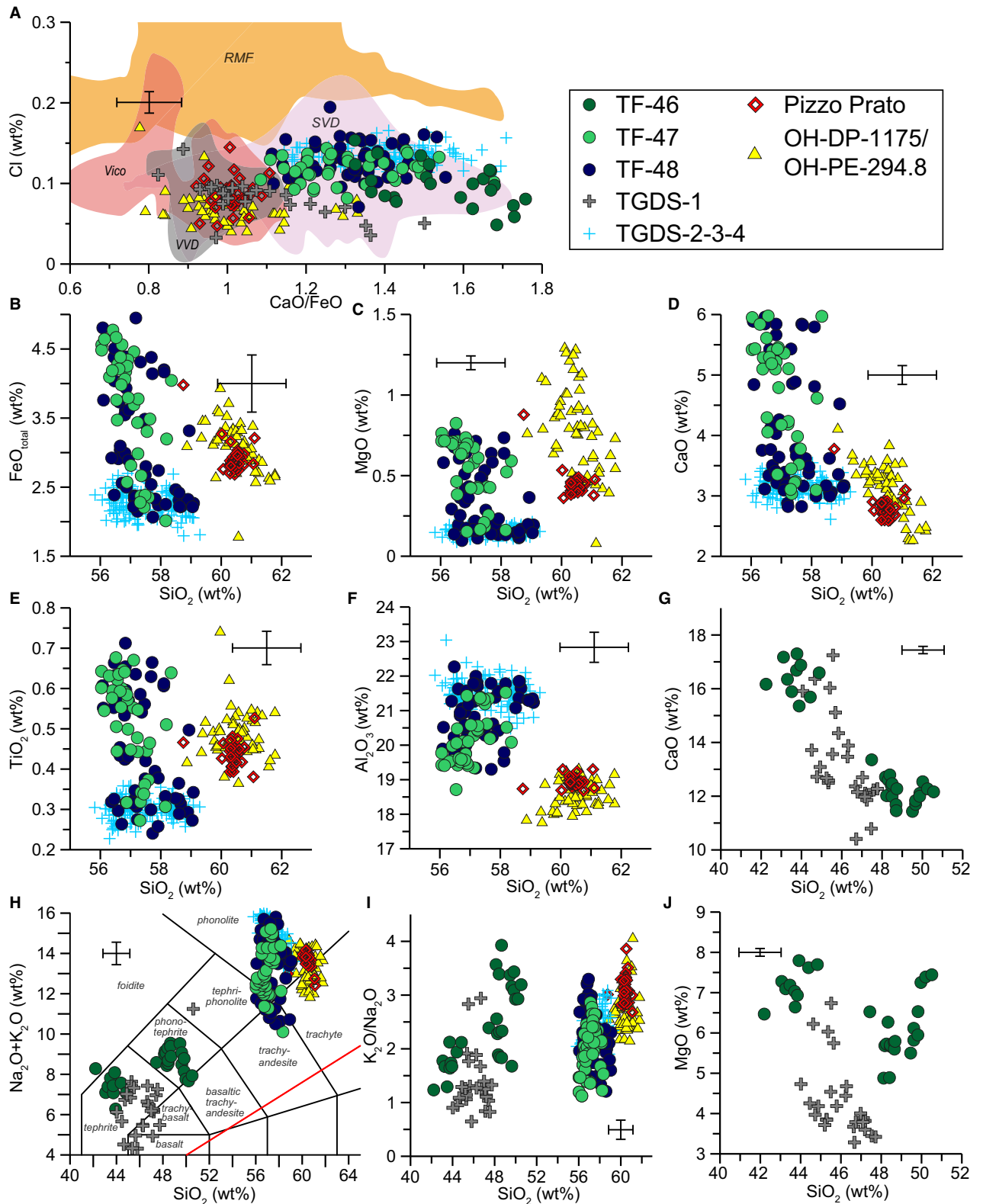
Fig. 4. TAS diagram and bi-variate plots of tephra layers associated with the SVD. A, H, I. The full compositional spectrum of tephra layers TF-46-/-47-/48 is shown together with potential equivalents from the SVD (new data of this study TGDS1-4 and TGdS data (from TGDS2-4) based on Giaccio *et al.* (2019) and Pizzo Prato data from Monaco *et al.* (2022a)) and the Lake Ohrid record (data from Leicher *et al.* (2021) and Wagner *et al.* (2023)). B, C, D, E, F. Bi-variate plots of compared tephra layers with SiO₂ composition >56 wt%. G, J. Bi-variate plots of compared tephra layers with SiO₂ composition <52 wt%. TAS classification according to Le Bas *et al.* (1986) and CaO/FeO vs. Cl diagram based on Giaccio *et al.* (2017b). Error bars represent the twofold standard deviation of replicate analyses of ATHO-G.
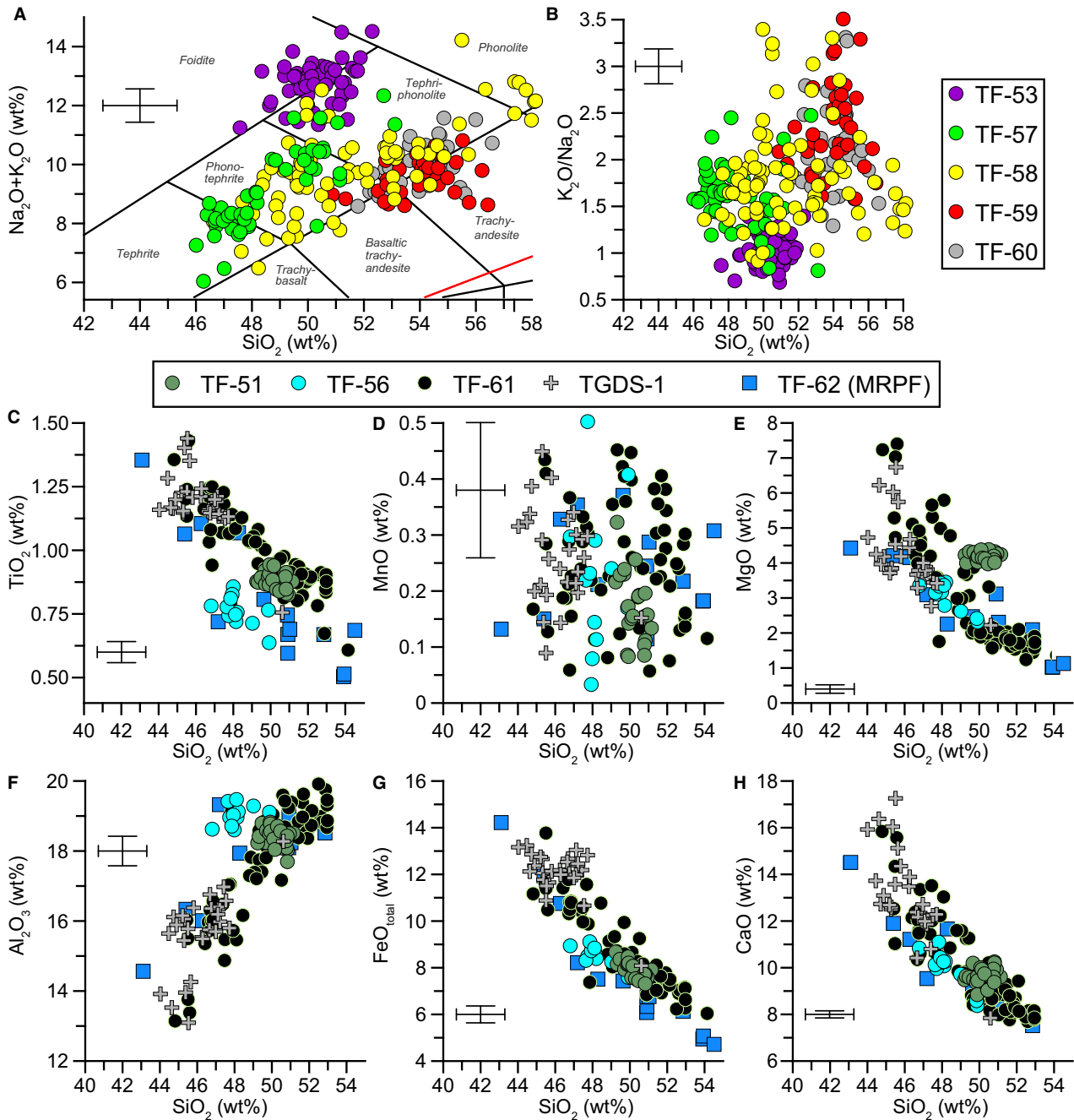
Fig. 5. TAS diagram and bi-variate plots of tephra layers associated with the SVD and undefined Roman origin. A, B. Comparison of tephra layers TF-53/-57/-58/-59/-60. C–H. Comparison of TF-51/-56/-61 and Unit 1 of the TGdS (data based on Giaccio *et al.* (2019) and new data of this study) and the MRPF (data from Leicher *et al.* (2022)). Error bars represent the twofold standard deviation of replicate analyses of ATHO-G.

analyses plotting in the field of the VVD of the CaO/FeO vs. Cl diagram (Fig. 3). TF-61 was $^{40}Ar/^{39}Ar$ dated at 313.3±1.0 ka and is thus within the given age uncertainties statistically synchronous with the directly underlying TF-62 (313.5±1.4 ka, Table 1), which is correlated with the MRPF eruption of the SVD (Leicher *et al.* 2022). Redeposition of TF-62 can be excluded, as TF-61 has different lithological and geochemical

properties with a distinct threefold zonation. TF-62 also includes a dominating phonolitic composition, which is not observed for TF-61, but their tephritic to tephriphonolitic compositions overlap (Fig. 5C–H). Based on geochemical and chronological similarities TF-61 most likely represents a post-MRPF eruptive event, which occurred less than a millennium after the main eruption.

Vulsini volcanic district (VVD) tephra

TF-59/-60 (modelled ages 311.7±2.3, 311.9±2.3 ka). –
Tephra layers TF-59 and TF-60 both have a -
phonotephritic-tephriphonolitic-trachyandesitic compo-
sition with mean alkali ratios of 2.4 and 2.2, respectively.
Based on the CaO/FeO vs. Cl diagram TF-59/-60 both
have a supposed origin from the VVD or Vico volcano
(Fig. 3D). For the Vico volcano no explosive activity at
that time is reported (Perini *et al.* 2004), whereas from the
VVD the Orvieto–Bagnoregio (WOB) is the main
eruption known for the time frame at *c.* 300–340 ka
(Marra *et al.* 2020b). The WOB eruption was identified
within the F4-F5 succession (TF-69; 331.5±2.2 ka) as
well as in proximal archives together with a series of post-
(322–329 ka) and pre- (*c.* 339 ka) eruptive events (Marra
et al. 2020b; Leicher *et al.* 2022). A very minor $^{40}Ar/^{39}Ar$
age population of *c.* 314±7 ka (CB4/5, *n* = 3) identified
within the proximal deposits (Marra *et al.* 2020b) sup-
ports that TF-59/-60 may represent minor, still unknown
eruptive events of the VVD.

Colli Albani volcanic (CAVD) tephra

TF-53 (modelled age 301.0±3.6 ka). – Tephra TF-53
has a dominantly foiditic-tephriphonolitic composition
with some minor phonolitic components and alkali
ratios between 0.7–1.5. TF-53 plots in both the SVD and
Roccamonfina fields (Fig. 3D), whereas foiditic compo-
sitions are rather known from the CAVD (Marra
et al. 2003; Boari *et al.* 2009a; Giaccio *et al.* 2013).
From the CAVD the crater forming event causing the
Castiglione maar succession has an estimated age of
c. 285 ka (Marra *et al.* 2003), thus being much younger.
Therefore, TF-53 is most likely related to the generic
explosive activity of the Faete phase leaving a precise
correlation to a specific eruption pending.

Roman tephra with mixed SVD/VVD compositions

Tephra layers TF-54, TF-57 and TF-58 have a compo-
sitional spectrum in the TAS diagram ranging from
tephrites to phonolites. This heterogeneous composition
is also expressed in their overlapping position within the
CaO/FeO vs. Cl diagram, occupying the fields of the
Roman volcanic districts Sabatini, Vulsini and Vico. In
addition to uncertainties concerning the precision of the
data themselves, the CaO/FeO ratio itself is less
distinctive for this compositional range, as also the data
defining the composition fields within the diagram
suggest a natural overlap in the composition of the three
Roman volcanoes.

For the Vico volcano only effusive products for the
time interval 305–258 ka are known (Perini *et al.* 2004),
and compositions related to older and younger explosive
events are of more evolved character following a
phonolitic-trachytic-rhyolitic evolution (Pereira *et al.*

2020; Monaco *et al.* 2021, 2022a). The F4-F5 tephra
layers form two age groups 302 ka (TF-54) and 310–
312 ka (TF-57/TF-58), for which potential eruptive
equivalents of the SVD and VVD are discussed below.

TF-54 (modelled age 301.8±3.5 ka). – TF-54 has a
tephriphonolitic-phonotephritic composition with some
minor phonolitic components, and a mean alkali ratio of
1.4. The position within the CaO/FeO vs. Cl diagram
plots both in the SVD and VVD fields, with a tendency
towards lower, VVD-like, CaO/FeO ratios. For TF-54 a
potential eruptive equivalent is the Case Pisello eruption
of the VVD, dated at 293.8±4.0 ka (Brocchini
et al. 2000).

TF-57/-58 (modelled ages 309.5±2.7, 310.5±2.6 ka). –
Tephra TF-57 has a tephritic-phonotephritic-
tephriphonolitic composition, whereas the composition
of TF-58 also includes phonolitic components with mean
alkali ratios of 1.6 and 1.9, respectively. Based on their
close position to the underlying MRPF deposits, these
tephra layers were tentatively related to the post volcanic
activity within the SVD, as no dated explosive activity has
been reported for the VVD so far (Marra *et al.* 2020b).
TF-58 is the thicker (7 cm) of the two tephra layers and
likely represents a major eruptive event. Similar to the
other SVD-like tephra layers (TF-56, -61) the specific
origin from within the SVD cannot fully be resolved at
present. Besides the geochemical and chronological
similarities to the MRPF, the ages of the Fucino tephra
layers overlap with the youngest age of the Tufo die
Bracciano eruption (310.0±5.0 ka; Sottili *et al.* 2010).
Indications of contemporaneous volcanic activity are also
found in palaeo-surfaces from the Tyrrhenian coastal
area, where an unknown volcanic event is dated at
310.2±4.3 ka (KW-1; Marra *et al.* 2023).

Roccamonfina tephra

TF-55 (modelled age 303.6±3.4 ka). – TF-55 has a
phonolitic-trachytic composition with a low alkali ratio
(mean = 0.8) and low CaO values (mean = 1.0 wt%).
Its position within the CaO/FeO vs. Cl diagram plots is
in the field of Ischia; however, Ischia's known volcanic
activity only dates back to 150 ka (Sbrana *et al.* 2018).
Glass compositions similar to TF-55 have been observed
for tephra layers TF-64 and TF-64a (*c.* 316 ka), which
are correlated with the volcanic products of the White
Trachytic Tuff (WTT) Unit D of the Roccamonfina
volcano (312.9±4.0 ka; Giannetti & De Casa 2000;
Leicher *et al.* 2022). The younger WTT Unit E has
besides its basal unit (UE) three distinct subunits (E1–3),
of which E1 was imprecisely dated in proximal deposits
between 301 and 310 ka (Giannetti & De Casa 2000)
and correlated with an ash layer of the Bojano basin
(312.1±5.0 ka; Amato *et al.* 2014; Leicher *et al.* 2022).
However, the composition of E1 together with that of the

undated WTT units UE and E2 only partially overlap with TF-55 (Fig. 6), as they have a generally more evolved trachytic character. For the younger Unit E3 (301.5±8.0 ka) and Unit F (292.5±14.0 ka) of the WTT no glass geochemical data are available, but these are the best potential equivalents from a temporal perspective. However, Ballini *et al.* (1991) described less evolved compositions for the younger WTT deposits. This is also observed for tephra layers found in the Lake Ohrid succession (OH-DP-0997/-1055: *c.* 230–241 ka; Leicher *et al.* 2019), which are related to the younger WTT

activity and are supposed to have similar compositions to TF-55. Therefore, TF-55 most likely represents an equivalent of the WTT series, whose exact correlation with one of the subunits still needs to be verified.

The 250–315 ka explosive history of Italian volcanism inferred from the Fucino record

The investigations of the volcanic sources of the tephra layers identified in the F4-F5 site confirm the general pattern of volcanic activity observed in proximal settings
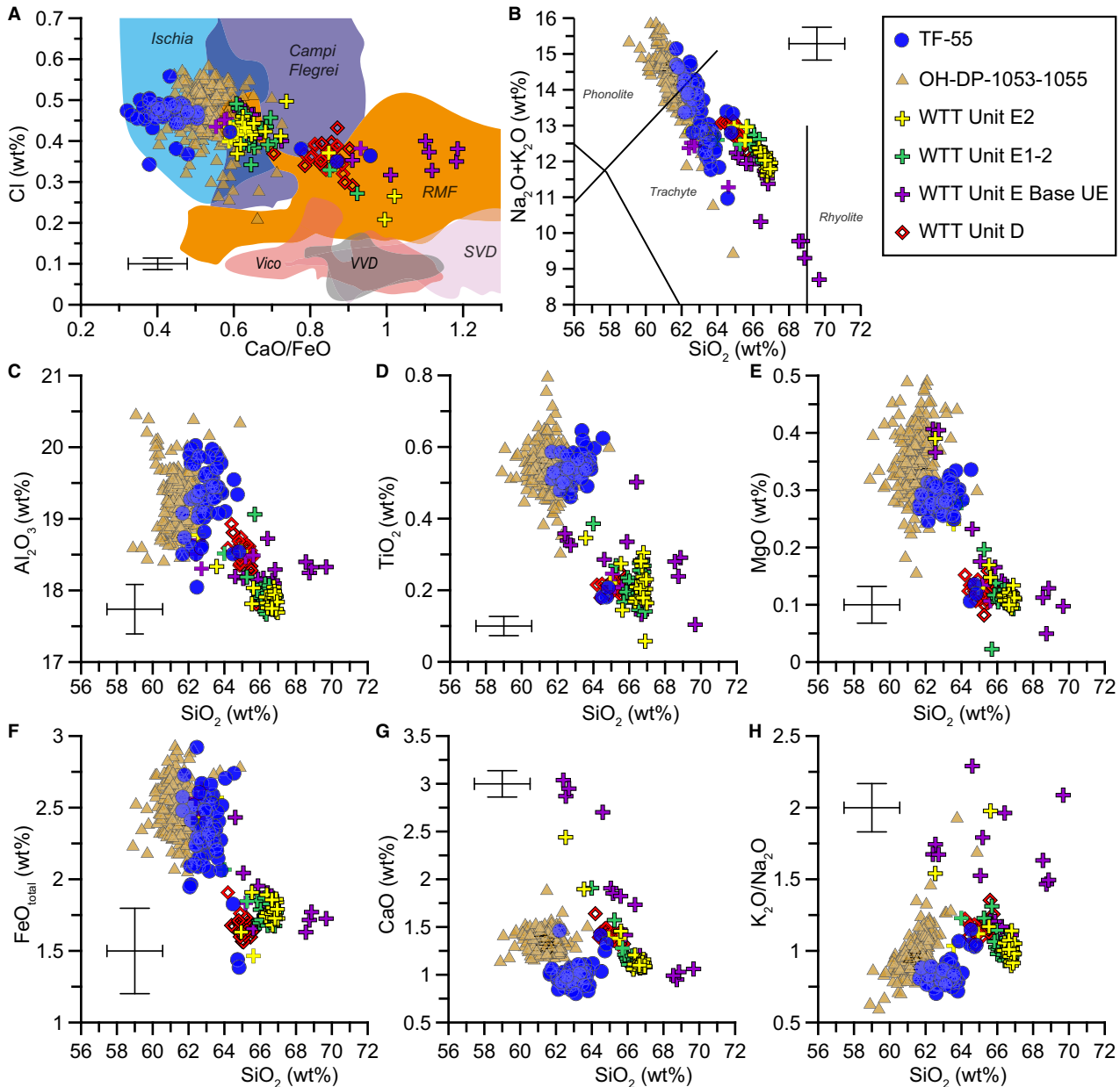

Fig. 6. TAS diagram and bi-variate plots of tephra layers associated with the WTT of the Roccamonfina volcano and younger Roccamonfina products from the Lake Ohrid succession. A–H. Comparison of TF-55 with compositions of WTT Units D, E Base UE, E1-2 and E2 from Leicher *et al.* (2022) and tephra layers OH-DP-1053/-1055 from the Lake Ohrid succession (Leicher*et al.* 2021), which represent younger products (*c.* 230–245 ka) of the Roccamonfina WTT stage. Error bars represent the twofold standard deviation of replicate analyses of ATHO-G.

with a dominating influence of the Roman volcanoes (Fig. 7). The majority of tephra layers (*n* = 10) of the F4-F5 succession likely originates from the SVD. Two of those can be confidently correlated with known major explosive events (Sottili *et al.* 2010, 2019) of the Magliano Romano Plinian Fall (TF-62; Leicher *et al.* 2022) and the Tufo Giallo di Sacrofano eruption (TF-48). Directly above the tephra equivalent of the MRPF eruption (TF-62), a cluster of four tephra layers (TF-56/-57/-58/-61) suggest by the narrow time interval of their deposition between 308.5±2.8 and 313.3±1.0 ka and the similarities in their geochemical signature an

alignment with the post-MRPF volcanic activity. However, also a correlation of TF-58 with the Tufo di Bracciano (TdB) is possible from a chronological perspective, as the youngest age obtained for the TdB is 310.0±5.0 ka (Sottili *et al.* 2010). The TdB is a major eruptive event with a widespread dispersal of a thick pyroclastic succession (Sottili *et al.* 2010), for which two clusters of ages exist (Sottili *et al.* 2010; Pereira *et al.* 2017). The younger age cluster at 310.0±5.0 ka (Sottili *et al.* 2010) is potentially represented by TF-58, a 7-cm-thick tephra representing a larger eruptive event, whereas the older cluster at 319.1±6.0 to 323.9±2.0 ka
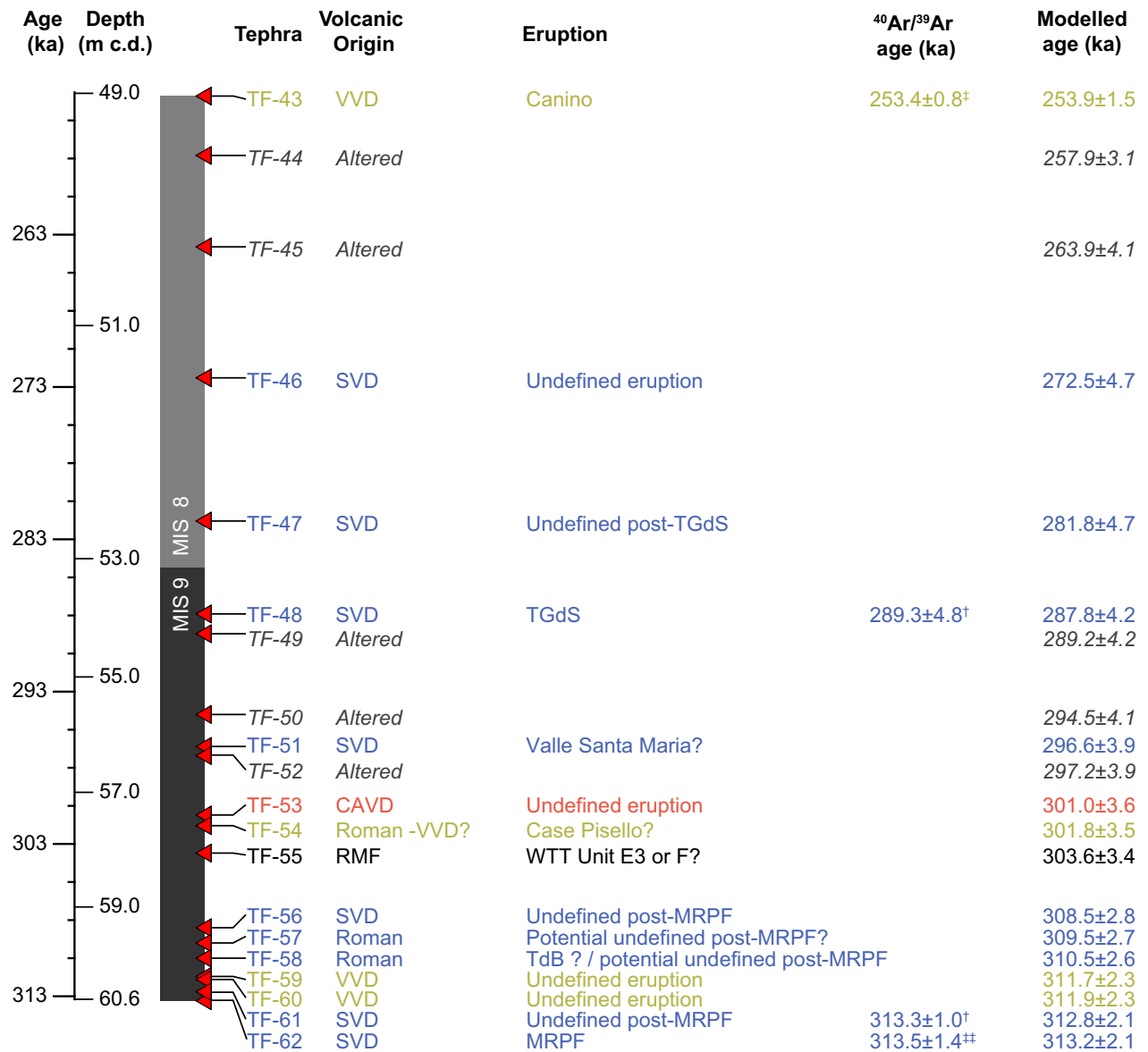

Fig. 7. Overview of the volcanic sources and chronology (^{40}Ar/^{39}Ar and modelled ages) of the investigated tephra layers within the Fucino F4-F5 record. The climatostratigraphical position of tephra layers is indicated by the MIS boundaries based on Lisiecki and Raymo (2005). Tephra layers are colour coded according to their supposed volcanic origin: VVD = Vulsini volcanic district (yellow); SVD = Sabatini Volcanic district (blue); CAVD = Colli Albani volcanic district (red); RMF = Roccamonfina volcano (black); tephra layers written in italics represent altered material; † = ^{40}Ar/^{39}Ar ages of this study; ‡ = ^{40}Ar/^{39}Ar age from Monaco *et al.* (2022a); ‡‡ = ^{40}Ar/^{39}Ar age from Leicher *et al.* (2022).

(Sottili *et al.* 2010; Pereira *et al.* 2017) is tentatively correlated with TF-65a (325.3±3.1 ka; Leicher *et al.* 2022) from the F4-F5 succession. Nevertheless, the cluster of tephra layers (TF-56/-57/-58/-61) suggest that either the MRPF and/or the Tufo di Bracciano events were followed by a series of eruptive events, which lasted for at least five millennia. Even though geochemical data sets of potential proximal equivalents are not available for comparison yet, these findings suggest that the known Strombolian and subordinately hydromagmatic eruptions during the waning phases of the Sacrofano and Bracciano calderas may have started already at *c.* 313 ka and thus earlier as previously suggested at *c.* 300 ka (Sottili *et al.* 2019). Another volcanic event of the SVD identified in the Fucino record, TF-51 (*c.* 297 ka), is potentially related to one of the minor explosive events of the Valle Santa Maria Maar (293.2±4.7 ka; Marra *et al.* 2020a).

The Fucino TGdS equivalent, i.e. TF-48, is $^{40}Ar/^{39}Ar$ dated at 289.3±4.8 ka, which represents a more precise age compared to that obtained for proximal deposits (288.8±6.0 ka; Sottili *et al.* 2010). Following the TF-48/TGdS eruption two tephra layers (TF-47: 281.8±4.7 ka and TF-46: 272.5±4.9 ka) of the SVD are identified, which suggest a longer paucity and lower frequency of post-TGdS activity compared to the post-MRPF activity. The composition of TF-47 is quite similar to that of TF-48, which is also different compared to the post-MRPF eruptions with low evolved compositions.

Another major eruptive event of the SVD, the Pizzo Prato eruption (251.4±16.0 ka; Sottili *et al.* 2010), is not found within the Fucino sediment succession. It was identified in the Lake Ohrid succession (OH-DP-1175), with an older, but more precise age of 270.6±4.9 ka (Leicher *et al.* 2021) according to the age model. As Lake Ohrid is located >700 km apart from the SVD, the lack of evidence in the F4-F5 record is surprising, especially because of the presence of the numerous minor SVD eruptions identified. Unfavourable preservation conditions in the Fucino succession are unlikely, as TF-46 is of similar age and related to the SVD. This may suggest a more southern and curved dispersal axis for the main Pizzo Prato phase. The different composition of TF-46 compared with the composition of the main Pizzo Prato event suggests it to represent either a different phase of the eruption or a pre/post eruptive event.

Besides the previously identified Canino eruption (TF-43: 253.4±0.8 ka; Monaco *et al.* 2022a), three other tephra layers of the F4-F5 record are related to the activity of the VVD. TF-59/-60 are undefined eruptive events with an age of 311.7–311.9±2.2 ka, which are potentially also recorded in the youngest age cluster of CB4/5 in proximal deposits (Marra *et al.* 2020a). Tephra TF-54 (301.8±3.5 ka) is tentatively associated with the Case Pisello eruption, which was dated at 293.8±4.0 ka (Brocchini *et al.* 2000). The absence of further VVD-like tephra layers between *c.* 253 and 302 ka in the F4-F5 record confirms the lack of major explosive events from the VVD during this period observed in its direct vicinity (Brocchini *et al.* 2000; Palladino *et al.* 2010; Marra *et al.* 2020b).

Tephra layer TF-53 (301.0±3.6 ka) was associated with the explosive volcanic activity of the Delle Faete phase (*c.* 250–308 ka; Marra *et al.* 2003) of the CAVD; however, a correlation with a specific eruption is pending.

Within the studied succession, only one tephra indicates an origin from the Roccamonfina volcano. Tephra TF-55 (303.6±3.4 ka) is associated with the White Trachytic Tuff, but a robust correlation with one of the subunits of WTT E or F is pending at present. However, also for the older WTT equivalents, identified in the section below (Leicher *et al.* 2022), a straightforward correlation with one of the proximal subunits was challenging, indicating the need for further detailed geochemical and chronostratigraphical investigations of the proximal deposits.

The 250–315 ka Fucino record in the tephrostratigraphical framework of the central Mediterranean

So far, the central Mediterranean tephrostratigraphical framework for the interval 250–315 ka was based on fragmentary information from the Italian Peninsula. Information derived from continuous stratigraphical succession covering the entire interval was only provided by distal archives, which may record only the most widespread eruptions. At present, the Fucino F4-F5 record from central Italy provides the most detailed and well-dated succession providing 20 volcanic events for this interval (Fig. 7) and can act as a reference section to improve correlations between different archives.

Mediterranean sedimentary archives for which tephra layers within the investigated time frame have been reported are the Italian San Gregorio Magno (Munno &

Fig. 8. Synthesis of proximal and distal information of the volcanic history of the Italian volcanoes and the resulting tephrostratigraphical framework of the central Mediterranean region. All $^{40}Ar/^{39}Ar$ ages from literature were recalculated according to ACs at 1.1891 Ma (Niespolo *et al.* 2017) and the total K decay constant of Renne *et al.* (2011). See also Table 2 for references and ages. The ages of tephra layers from the distal records are based on archive specific age-depth models (Lourens 2004; Piva *et al.* 2008; Vakhrameeva *et al.* 2019; Leicher *et al.* 2021). Data for the LR04 are based on Lisiecki & Raymo (2005) with the MIS substages of Railsback *et al.* (2015). XRF data of the Lake Ohrid DEEP site from Wagner (2019). The column 'Synthesis of Italian volcanic activity' combines all information. If robust correlations of equivalent eruptive events could be established and several ages were available, only the most reliable age is shown as discussed in the respective subsection.
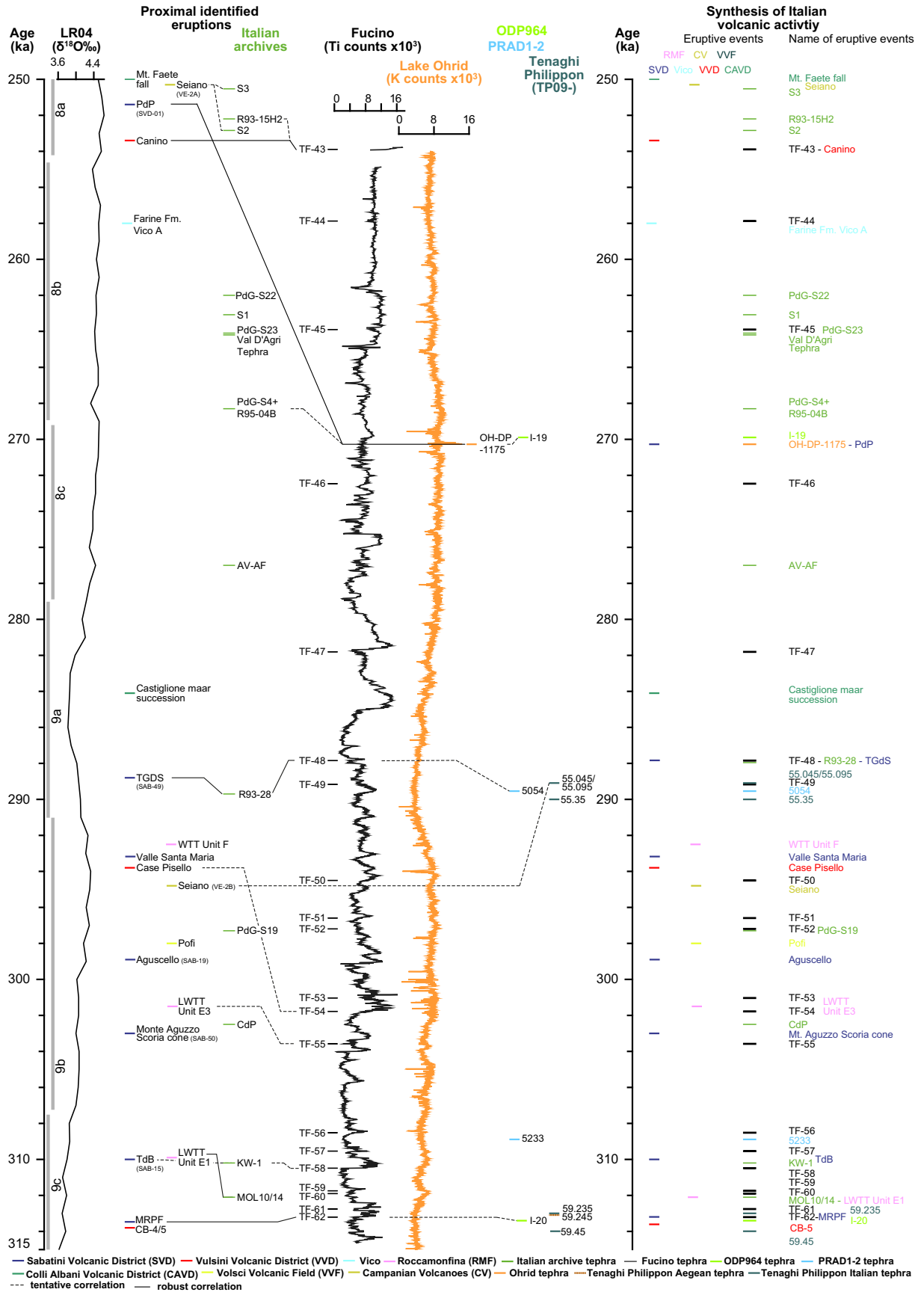
Petrosino 2007) and Bojano basins (Amato *et al.* 2014), outcrops along the Tiber river and its tributaries (Marra *et al.* 2016, 2018, 2023), the marine records of KC01B/ODP964A+B (Lourens 2004) and PRAD1-2 (Piva *et al.* 2008), and the terrestrial records from Lake Ohrid (Leicher *et al.* 2021) and Tenaghi Philippon (Vakhrameeva *et al.* 2019) (cf. Fig. 1A). A tephrostratigraphical overview combining distal archives and near-vent volcanic records is provided in Fig. 8.

The oldest tephra layers (S1–S4, Campanian or Roccamonfina origin) found in the San Gregorio Magno basin (Munno & Petrosino 2007) have an estimated age between *c.* 241–263 ka (Ascione *et al.* 2013), but no equivalent tephra could be recognized in the Fucino record. Furthermore, the integration of 10 volcanic events dated in the different outcrops of the Tiber valley and its tributaries (Marra *et al.* 2016, 2018, 2023) can only be conducted from a chronological perspective, since geochemical data are not available. However, this would be of particular interest as these deposits were used to reconstruct sea-level changes (Marra *et al.* 2016, 2023) and thus would provide tie points for the alignment with other palaeoenvironmental records. Some of these tephra ages overlap with the (undefined) eruptions identified within the F4-F5 record, such as the volcanoclastic deposits PdG-13 (247.3±3.9 ka; Marra *et al.* 2016) and R93-15H2 (252.2±8.0 ka; Marra *et al.* 2016) with the Canino equivalent TF-43 (253.4±0.8 ka). Besides the identification of the Pizzo Prato eruption in the Lake Ohrid succession (OH-DP-1175; Leicher *et al.* 2019), it also might be represented by PdG-S4+R95-04B (268.3±3.8 ka; Marra *et al.* 2016). AV-AF (277.0±1.6 ka; Marra *et al.* 2016) has a similar age to that of the altered tephra layers TF-46 and TF-47. The Tufo Giallo di Sacrofano eruption (TF-48; 289.3±4.8 ka) was also identified within the Roman area (R93-28: 289.7±2.0 ka; Karner & Renne 1998; Marra *et al.* 2016). Tephra layers TF-51/-55 (297–302 ka) arise as potential equivalents of PdG-S19 (297.3±2.2 ka; Marra *et al.* 2016) and CdP (302.5±9.0 ka; Marra *et al.* 2018).

In marine records, tephra layers I-19 (*c.* 270 ka, potential Pizzo Prato) and I-20 (*c.* 313 ka, potential MRPF) were described in cores from the Ionian Sea (KC01B/ODP964A+B; Lourens 2004), but investigations for obtaining their geochemical composition were not successful (Vakhrameeva *et al.* 2021). Further, two tephra layers (PRAD5054: *c.* 290 ka and PRAD5233: *c.* 309 ka) identified in the PRAD1-2 record from the Adriatic Sea (Piva *et al.* 2008) represent potential equivalents from a chronological perspective of the TGdS (TF-48) and the post-MRPF activity identified in the Fucino succession (TF-56-TF-61). From the Tenaghi Philippon peat record in Greece, at least five tephra layers of Italian origin were identified between 289–315 ka, but their compositions suggest an origin from either the Neapolitan or Aeolian Arc volcanoes, thus differing from the tephra layers of the Fucino record.

Conclusions

Lithological, geochemical and chronological characteristics of 13 tephra layers identified in the MIS 8/9 interval of the Fucino F4-F5 sediment succession were investigated aiming at assessing their volcanic sources. Single crystal $^{40}Ar/^{39}Ar$ ages of four tephra layers set the basis for a Bayesian age-depth model for the interval 250–315 ka, which enabled indirect dating of the other tephra layers within the succession through interpolation. The investigation of this interval completes the tephrostratigraphical and tephrochronological investigations of macroscopic tephra layers of the F4-F5 sediment succession, which represents the first continuous and most tephra rich sediment succession of the last 425 ka within the central Mediterranean region. Identifying the volcanic sources and, in some cases, the specific equivalent eruptions or eruptive phases provides new insights into the eruptive history of Italian volcanism. This applies in particular to the major known eruptions of the Sabatini and Vulsini volcanic districts of the Roman Province and the Roccamonfina volcano.

The established tephrostratigraphy of the stratigraphically ordered Fucino succession represents a reference data set for reassessing the order and chronology of (minor) eruptive events not yet conclusively identified in proximal settings. It is also a key section for the subsequent extension of the central Mediterranean tephrostratigraphical framework for this period, which previously lacked a continuous sequence in close proximity to the volcanic sources. Similar to the tephrostratigraphical observations made for the F4-F5 record before, the amount of so far unidentified eruptive events suggests the need for further detailed investigations of near-vent successions. This would help to improve the geochemical and geochronological data basis especially for eruptions of lower magnitude, but highlights also the need for cryptotephra analysis of distal records, to link the available archives.

10.26022/IEDA/112832. The XRF data that support the findings of this study are available from the corresponding author upon reasonable request. ^{40}Ar/^{39}Ar original data are available in Table S1.

References

Albert, P. G., Giaccio, B., Isaia, R., Costa, A., Niespolo, E. M., Nomade, S., Pereira, A., Renne, P. R., Hinchliffe, A., Mark, D. F., Brown, R. J. & Smith, V. C. 2019: Evidence for a large-magnitude eruption from Campi Flegrei caldera (Italy) at 29 ka. *Geology 47*, 595–599.

Amato, V., Aucelli, P. P. C., Cesarano, M., Jicha, B., Lebreton, V., Orain, R., Pappone, G., Petrosino, P. & Ermolli, E. R. 2014: Quaternary evolution of the largest intermontane basin of the Molise Apennine (central-southern Italy). *Rendiconti Lincei 25*, 197–216.

Ascione, A., Mazzoli, S., Petrosino, P. & Valente, E. 2013: A decoupled kinematic model for active normal faults: insights from the 1980, MS = 6.9 Irpinia earthquake, southern Italy. *Geological Society of America Bulletin 125*, 1239–1259.

Ballini, A., Barberi, F., Laurenzi, M. A., Mezzetti, F., Oddone, M. & Villa, I. M. 1991: Chrono-stratigraphy of Roccamonfina volcanic complex. *Plinius 4*, 35–36.

Blaauw, M. & Christen, J. A. 2011: Flexible paleoclimate age-depth models using an autoregressive gamma process. *Bayesian Analysis 6*, 457–474.

Boari, E., Avanzinelli, R., Melluso, L., Giordano, G., Mattei, M., De Benedetti, A. A., Morra, V. & Conticelli, S. 2009a: Isotope geochemistry (Sr–Nd–Pb) and petrogenesis of leucite-bearing volcanic rocks from "Colli Albani" volcano, Roman Magmatic Province, Central Italy: inferences on volcano evolution and magma genesis. *Bulletin of Volcanology 71*, 977–1005.

Boari, E., Tommasini, S., Laurenzi, M. A. & Conticelli, S. 2009b: Transition from ultrapotassic kamafugitic to sub-alkaline magmas: Sr, Nd, and Pb isotope, trace element and ^{40}Ar–^{39}Ar age data from the Middle Latin Valley Volcanic Field, Roman Magmatic Province, Central Italy. *Journal of Petrology 50*, 1327–1357.

Brocchini, D., Di Battistini, G., Laurenzi, M. A., Vernia, L. & Bargossi, G. M. 2000: New ^{40}Ar/^{39}Ar datings on the southeastern sector of the Vulsinian volcanic district. *Italian Journal of Geosciences 119*, 113–120.

Cardello, G. L., Consorti, L., Palladino, D. M., Carminati, E., Carlini, M. & Doglioni, C. 2020: Tectonically controlled carbonate-seated maar-diatreme volcanoes: the case of the Volsci Volcanic Field, central Italy. *Journal of Geodynamics 139*, 101763, https://doi.org/10.1016/j.jog.2020.101763.

Cavinato, G. P., Carusi, C., Dall'Asta, M., Miccadei, E. & Piacentini, T. 2002: Sedimentary and tectonic evolution of Plio–Pleistocene alluvial and lacustrine deposits of Fucino Basin (central Italy). *Sedimentary Geology 148*, 29–59.

D'Addezio, G., Karner, D. B., Burrato, P., Insinga, D., Maschio, L., Ferranti, L. & Renne, P. R. 2006: Tephrochronology in faulted Middle Pleistocene tephra layer in the Val d'Agri area (Southern Italy). *Annales Geophysicae 49*, 1029–1040.

D'Agostino, N., Jackson, J. A., Dramis, F. & Funiciello, R. 2001: Interactions between mantle upwelling, drainage evolution and active normal faulting: an example from the central Apennines (Italy). *Geophysical Journal International 147*, 475–497.

De Rita, D., Funiciello, R. & Parotto, M. 1988: *Geological map of the Colli Albani volcanic complex*. Progetto Finalizzato Geodinamica CNR, Rome, Italy.

Del Carlo, P., Smedile, A., Petrelli, M. & Di Roberto, A. 2020: Evidence for an unknown explosive eruption of Mt. Etna volcano (Italy) during the Late Glacial. *Journal of Volcanology and Geothermal Research 402*, 106992, https://doi.org/10.1016/j.jvolgeores.2020.106992.

Di Roberto, A., Smedile, A., Del Carlo, P., De Martini, P. M., Iorio, M., Petrelli, M., Pantosti, D., Pinzi, S. & Todrani, A. 2018: Tephra and cryptotephra in a ~ 60,000-year-old lacustrine sequence from the Fucino Basin: new insights into the major explosive events in Italy.

Bulletin of Volcanology 80, 20, https://doi.org/10.1007/s00445-018-1200-x.

Galadini, F. & Galli, P. 2000: Active tectonics in the Central Apennines (Italy) – input data for seismic hazard assessment. *Natural Hazards 22*, 225–268.

Giaccio, B., Arienzo, I., Sottili, G., Castorina, F., Gaeta, M., Nomade, S., Galli, P. & Messina, P. 2013: Isotopic (Sr-Nd) and major element fingerprinting of distal tephras: an application to the Middle-Late Pleistocene markers from the Colli Albani volcano, central Italy. *Quaternary Science Reviews 67*, 190–206.

Giaccio, B., Galli, P., Messina, P., Peronace, E., Scardia, G., Sottili, G., Sposato, A., Chiarini, E., Jicha, B. & Silvestri, S. 2012: Fault and basin depocentre migration over the last 2 Ma in the L'Aquila 2009 earthquake region, central Italian Apennines. *Quaternary Science Reviews 56*, 69–88.

Giaccio, B., Hajdas, I., Isaia, R., Deino, A. & Nomade, S. 2017a: High-precision 14C and ^{40}Ar/^{39}Ar dating of the Campanian Ignimbrite (Y-5) reconciles the time-scales of climatic-cultural processes at 40 ka. *Scientific Reports 7*, 45940, https://doi.org/10.1038/srep45940.

Giaccio, B., Leicher, N., Mannella, G., Monaco, L., Regattieri, E., Wagner, B., Zanchetta, G., Gaeta, M., Marra, F., Nomade, S., Palladino, D. M., Pereira, A., Scheidt, S., Sottili, G., Wonik, T., Wulf, S., Zeeden, C., Ariztegui, D., Cavinato, G. P., Dean, J. R., Florindo, F., Leng, M. J., Macri, P., Niespolo, E., Renne, P. R., Rolf, C., Sadori, L., Thomas, C. & Tzedakis, P. C. 2019: Extending the tephra and palaeoenvironmental record of the Central Mediterranean back to 430 ka: a new core from Fucino Basin, central Italy. *Quaternary Science Reviews 225*, 106003, https://doi.org/10.1016/j.quascirev.2019.106003.

Giaccio, B., Niespolo, E. M., Pereira, A., Nomade, S., Renne, P. R., Albert, P. G., Arienzo, I., Regattieri, E., Wagner, B., Zanchetta, G., Gaeta, M., Galli, P., Mannella, G., Peronace, E., Sottili, G., Florindo, F., Leicher, N., Marra, F. & Tomlinson, E. L. 2017b: First integrated tephrochronological record for the last ~ 190 kyr from the Fucino Quaternary lacustrine succession, central Italy. *Quaternary Science Reviews 158*, 211–234.

Giaccio, B., Regattieri, E., Zanchetta, G., Nomade, S., Renne, P. R., Sprain, C. J., Drysdale, R. N., Tzedakis, P. C., Messina, P., Scardia, G., Sposato, A. & Bassinot, F. 2015a: Duration and dynamics of the best orbital analogue to the present interglacial. *Geology 43*, 603–606.

Giaccio, B., Regattieri, E., Zanchetta, G., Wagner, B., Galli, P., Mannella, G., Niespolo, E., Peronace, E., Renne, P. R., Nomade, S., Cavinato, G. P., Messina, P., Sposato, A., Boschi, C., Florindo, F., Marra, F. & Sadori, L. 2015b: A key continental archive for the last 2 Ma of climatic history of the central Mediterranean region: a pilot drilling in the Fucino Basin, central Italy. *Scientific Drilling 20*, 13–19.

Giannetti, B. 2001: Origin of the calderas and evolution of Roccamonfina volcano (Roman Region, Italy). *Journal of Volcanology and Geothermal Research 106*, 301–319.

Giannetti, B. & De Casa, G. 2000: Stratigraphy, chronology, and sedimentology of ignimbrites from the white trachytic tuff, Roccamonfina Volcano, Italy. *Journal of Volcanology and Geothermal Research 96*, 243–295.

Giannetti, B. & Luhr, J. F. 1983: The white trachytic tuff of Roccamonfina volcano (Roman region, Italy). *Contributions to Mineralogy and Petrology 84*, 235–252.

Giordano, G., De Benedetti, A., Diana, A., Diano, G., Esposito, A., Fabbri, M., Gaudioso, F., Marasco, F., Mazzini, I. & Miceli, M. 2010: Stratigraphy, volcano tectonics and evolution of the Colli Albani volcanic field. *In* Funiciello, R. & Giordano, G. (eds.): *The Colli Albani Volcano*, 43–97. Geological Society of London, London.

Giordano, G., De Benedetti, A. A., Diana, A., Diano, G., Gaudioso, F., Marasco, F., Miceli, M., Mollo, S., Cas, R. A. F. & Funiciello, R. 2006: The Colli Albani mafic caldera (Roma, Italy): stratigraphy, structure and petrology. *Journal of Volcanology and Geothermal Research 155*, 49–80.

Huebner, J. S. & Woodruff, M. E. 1985: Chemical compositions and critical evaluation of microprobe standards available in the Reston microprobe facility. *U. S. Geological Survey Open File Report 85-718*, 1–237.

Insinga, D. D., Tamburrino, S., Lirer, F., Vezzoli, L., Barra, M., De Lange, G. J., Tiepolo, M., Vallefuoco, M., Mazzola, S. & Sprovieri, M. 2014: Tephrochronology of the astronomically-tuned KC01B deep-sea core, Ionian Sea: insights into the explosive activity of the Central Mediterranean area during the last 200 ka. *Quaternary Science Reviews 85*, 63–84.

Jarosewich, E. 2002: Smithsonian microbeam standards. *Journal of Research of the National Institute of Standards and Technology 107*, 681–685.

Jochum, K. P. and 52 others 2006: MPI-DING reference glasses for in situ microanalysis: new reference values for element concentrations and isotope ratios. *Geochemistry Geophysics Geosystems 7*, 1525–2027.

Karner, D. B. & Renne, P. R. 1998: $^{40}Ar/^{39}Ar$ geochronology of Roman volcanic province tephra in the Tiber River valley: age calibration of middle Pleistocene sea-level changes. *Geological Society of America Bulletin 110*, 740–747.

Keller, J., Ryan, W. B. F., Ninkovich, D. & Altherr, R. 1978: Explosive volcanic activity in the Mediterranean over the past 200,000 yr as recorded in deep-sea sediments. *Geological Society of America Bulletin 89*, 591–604.

Kutterolf, S., Schindlbeck, J. C., Jegen, M., Freundt, A. & Straub, S. M. 2019: Milankovitch frequencies in tephra records at volcanic arcs: the relation of kyr-scale cyclic variations in volcanism to global climate changes. *Quaternary Science Reviews 204*, 1–16.

Lavigne, F., Degeai, J.-P., Komorowski, J.-C., Guillet, S., Robert, V., Lahitte, P., Oppenheimer, C., Stoffel, M., Vidal, C. M., Surono, Pratomo, I., Wassmer, P., Hajdas, I., Hadmoko, D. S. & de Belizal, E. 2013: Source of the great A.D. 1257 mystery eruption unveiled, Samalas volcano, Rinjani Volcanic Complex, Indonesia. *Proceedings of the National Academy of Sciences 110*, 16742–16747.

Le Bas, M. J. L., Maitre, R. W. L., Streckeisen, A. & Zanettin, B. 1986: A chemical classification of volcanic rocks based on the total alkali-silica diagram. *Journal of Petrology 27*, 745–750.

Leicher, N. 2021: EPMA-WDS settings for glass at University of Cologne – vol. 1. *In* I.E.D.A. (ed.): *Interdisciplinary Earth Data Alliance (IEDA), EarthChem*, https://doi.org/10.26022/IEDA/111986.

Leicher, N. & Giaccio, B. 2021: EPMA-WDS settings for glass at IGAG-CNR – vol. 1. *In* I.E.D.A. (ed.): *Interdisciplinary Earth Data Alliance (IEDA), EarthChem*, https://doi.org/10.26022/IEDA/111987.

Leicher, N., Giaccio, B., Pereira, A., Nomade, S., Monaco, L., Mannella, G., Galli, P., Peronance, E., Palladino, D. M., Sottili, G., Zanchetta, G. & Wagner, B. 2022: Central Mediterranean tephrochronology between 313 and 366 ka: new insights from the Fucino palaeolake sediment succession. *Boreas 52*, 240–271.

Leicher, N., Giaccio, B., Zanchetta, G., Sulpizio, R., Albert, P. G., Tomlinson, E. L., Lagos, M., Francke, A. & Wagner, B. 2021: Lake Ohrid's tephrochronological dataset reveals 1.36 Ma of Mediterranean explosive volcanic activity. *Scientific Data 8*, 231, https://doi.org/10.1038/s41597-021-01013-7.

Leicher, N., Giaccio, B., Zanchetta, G., Wagner, B., Francke, A., Palladino, D. M., Sulpizio, R., Albert, P. G. & Tomlinson, E. L. 2019: Central Mediterranean explosive volcanism and tephrochronology during the last 630 ka based on the sediment record from Lake Ohrid. *Quaternary Science Reviews 226*, 106021, https://doi.org/10.1016/j.quascirev.2019.106021.

Leicher, N., Monaco, L., Wulf, S. & Sottili, G. 2023: Glass geochemical composition of tephra layers of the interval 253-313 ka from the Fucino F4-F5 record and proximal equivalents - vol. 1. *In* I.E.D.A. (ed.): *Interdisciplinary Earth Data Alliance (IEDA), EarthChem*, https://doi.org/10.26022/IEDA/112832.

Lisiecki, L. E. & Raymo, M. E. 2005: A Pliocene-Pleistocene stack of 57 globally distributed benthic $\delta^{18}O$ records. *Paleoceanography 20*, PA1003, https://doi.org/10.1029/2004PA001071.

Lourens, L. J. 2004: Revised tuning of Ocean Drilling Program Site 964 and KC01B (Mediterranean) and implications for the $\delta^{18}O$, tephra, calcareous nannofossil, and geomagnetic reversal chronologies of the past 1.1 Myr. *Paleoceanography 19*, PA3010, https://doi.org/10.1029/2003PA000997.

Lowe, D. J. 2011: Tephrochronology and its application: a review. *Quaternary Geochronology 6*, 107–153.

Ludwig, K. R. 2009: Isoplot 3.70: a geochronological toolkit for Microsoft excel. *Berkeley Geochronology Center Special Publication 4*, 1–76.

Mannella, G., Giaccio, B., Zanchetta, G., Regattieri, E., Niespolo, E. M., Pereira, A., Renne, P. R., Nomade, S., Leicher, N., Perchiazzi, N. & Wagner, B. 2019: Palaeoenvironmental and palaeohydrological variability of mountain areas in the central Mediterranean region: a 190 ka-long chronicle from the independently dated Fucino palaeolake record (central Italy). *Quaternary Science Reviews 210*, 190–210.

Marra, F., Cardello, G. L., Gaeta, M., Jicha, B. R., Montone, P., Niespolo, E. M., Nomade, S., Palladino, D. M., Pereira, A., De Luca, G., Florindo, F., Frepoli, A., Renne, P. R. & Sottili, G. 2021: The Volsci Volcanic Field (central Italy): eruptive history, magma system and implications on continental subduction processes. *International Journal of Earth Sciences 110*, 689–718.

Marra, F., Castellano, C., Cucci, L., Florindo, F., Gaeta, M., Jicha, B. R., Palladino, D. M., Sottili, G., Tertulliani, A. & Tolomei, C. 2020a: Monti Sabatini and Colli Albani: the dormant twin volcanoes at the gates of Rome. *Scientific Reports 10*, 8666, https://doi.org/10.1038/s41598-020-65394-2.

Marra, F., Costantini, L., Di Buduo, G. M., Florindo, F., Jicha, B. R., Monaco, L., Palladino, D. M. & Sottili, G. 2019: Combined glacio-eustatic forcing and volcano-tectonic uplift: geomorphological and geochronological constraints on the Tiber River terraces in the eastern Vulsini Volcanic District (central Italy). *Global and Planetary Change 182*, 103009, https://doi.org/10.1016/j.gloplacha.2019.103009.

Marra, F., Freda, C., Scarlato, P., Taddeucci, J., Karner, D. B., Renne, P. R., Gaeta, M., Palladino, D. M., Trigila, R. & Cavarretta, G. 2003: Post-caldera activity in the Alban Hills volcanic district (Italy): $^{40}Ar/^{39}Ar$ geochronology and insights into magma evolution. *Bulletin of Volcanology 65*, 227–247.

Marra, F., Jicha, B., Palladino, D. M., Gaeta, M., Costantini, L. & Di Buduo, G. M. 2020b: $^{40}Ar/^{39}Ar$ single crystal dates from pyroclastic deposits provide a detailed record of the 590–240 ka eruptive period at the Vulsini Volcanic District (central Italy). *Journal of Volcanology and Geothermal Research 398*, 106904, https://doi.org/10.1016/j.jvolgeores.2020.106904.

Marra, F., Nomade, S., Pereira, A., Petronio, C., Salari, L., Sottili, G., Bahain, J. J., Boschian, G., Di Stefano, G., Falguères, C., Florindo, F., Gaeta, M., Giaccio, B. & Masotta, M. 2018: A review of the geologic sections and the faunal assemblages of Aurelian Mammal Age of Latium (Italy) in the light of a new chronostratigraphic framework. *Quaternary Science Reviews 181*, 173–199.

Marra, F., Rohling, E. J., Florindo, F., Jicha, B., Nomade, S., Pereira, A. & Renne, P. R. 2016: Independent $^{40}Ar/^{39}Ar$ and ^{14}C age constraints on the last five glacial terminations from the aggradational successions of the Tiber River, Rome (Italy). *Earth and Planetary Science Letters 449*, 105–117.

Marra, F., Sevink, J., Tolomei, C., Vannoli, P., Florindo, F., Jicha, B. R. & La Rosa, M. 2023: New age constraints on the MIS 9 – MIS 5.3 marine terraces of the Pontine Plain (central Italy) and implications for global sea levels. *Quaternary Science Reviews 300*, 107866, https://doi.org/10.1016/j.quascirev.2022.107866.

McGuire, A. M., Lane, C. S., Roucoux, K. H., Albert, P. G. & Kearney, R. 2022: The dating and correlation of an eastern Mediterranean lake sediment sequence: a 46–4 ka tephrostratigraphy for Ioannina (NW Greece). *Journal of Quaternary Science 37*, 1313–1331.

Monaco, L., Leicher, N., Palladino, D. M., Arienzo, I., Marra, F., Petrelli, M., Nomade, S., Pereira, A., Sottili, G., Conticelli, S., D'Antonio, M., Fabbrizio, A., Jicha, B. R., Mannella, G., Petrosino, P., Regattieri, E., Tzedakis, P. C., Wagner, B., Zanchetta, G. & Giaccio, B. 2022a: The Fucino 250–170 ka tephra record: new insights on peri-Tyrrhenian explosive volcanism, central mediterranean tephrochronology, and timing of the MIS 8-6 climate variability. *Quaternary Science Reviews 296*, 107797, https://doi.org/10.1016/j.quascirev.2022.107797.

Monaco, L., Palladino, D. M., Albert, P. G., Arienzo, I., Conticelli, S., Di Vito, M., Fabbrizio, A., D'Antonio, M., Isaia, R., Manning, C. J., Nomade, S., Pereira, A., Petrosino, P., Sottili, G., Sulpizio, R., Zanchetta, G. & Giaccio, B. 2022b: Linking the Mediterranean MIS 5 tephra markers to Campi Flegrei (southern Italy) 109–92 ka

explosive activity and refining the chronology of MIS 5c-d millennial-scale climate variability. *Global and Planetary Change 211*, 103785, https://doi.org/10.1016/j.gloplacha.2022.103785.

Monaco, L., Palladino, D. M., Gaeta, M., Marra, F., Sottili, G., Leicher, N., Mannella, G., Nomade, S., Pereira, A., Regattieri, E., Wagner, B., Zanchetta, G., Albert, P. G., Arienzo, I., D'Antonio, M., Petrosino, P., Manning, C. J. & Giaccio, B. 2021: Mediterranean tephrostratigraphy and peri-Tyrrhenian explosive activity revaluated in light of the 430-365 ka record from Fucino Basin (central Italy). *Earth-Science Reviews 220*, 103706, https://doi.org/10.1016/j.earscirev.2021.103706.

Mondati, G., Spadi, M., Gliozzi, E., Cosentino, D., Cifelli, F., Cavinato, G. P., Tallini, M. & Mattei, M. 2021: The tectono-stratigraphic evolution of the Fucino Basin (central Apennines, Italy): new insights from the geological mapping of its north-eastern margin. *Journal of Maps 17*, 87–100.

Munno, R. & Petrosino, P. 2007: The late Quaternary tephrostratigraphical record of the San Gregorio Magno basin (southern Italy). *Journal of Quaternary Science 22*, 247–266.

Niespolo, E. M., Rutte, D., Deino, A. L. & Renne, P. R. 2017: Intercalibration and age of the Alder Creek sanidine $^{40}Ar/^{39}Ar$ standard. *Quaternary Geochronology 39*, 205–213.

Palladino, D. M., Gaeta, M., Giaccio, B. & Sottili, G. 2014: On the anatomy of magma chamber and caldera collapse: the example of trachy-phonolitic explosive eruptions of the Roman Province (Central Italy). *Journal of Volcanology and Geothermal Research 281*, 12–26.

Palladino, D. M., Simei, S., Sottili, G. & Trigila, R. 2010: Integrated approach for the reconstruction of stratigraphy and geology of Quaternary volcanic terrains: an application to the Vulsini Volcanoes (Central Italy). *Geological Society of America Special Papers 464*, 63–84.

Patacca, E., Scandone, P., Di Luzio, E., Cavinato, G. P. & Parotto, M. 2008: Structural architecture of the central Apennines: interpretation of the CROP 11 seismic profile from the Adriatic coast to the orographic divide. *Tectonics 27*, TC3006, https://doi.org/10.1029/2005TC001917.

Paterne, M., Guichard, F., Duplessy, J. C., Siani, G., Sulpizio, R. & Labeyrie, J. 2008: A 90,000–200,000 yrs marine tephra record of Italian volcanic activity in the Central Mediterranean Sea. *Journal of Volcanology and Geothermal Research 177*, 187–196.

Peccerillo, A. 2005: *Plio-Quaternary Volcanism in Italy: Petrology, Geochemistry, Geodynamics.* 365 pp. Springer-Verlag, Berlin.

Peccerillo, A. & Frezzotti, M. L. 2015: Magmatism, mantle evolution and geodynamics at the converging plate margins of Italy. *Journal of the Geological Society 172*, 407–427.

Pereira, A., Monaco, L., Marra, F., Nomade, S., Gaeta, M., Leicher, N., Palladino, D. M., Sottili, G., Guillou, H., Scao, V. & Giaccio, B. 2020: Tephrochronology of the central Mediterranean MIS 11c interglacial (∼425–395 ka): new constraints from the Vico volcano and Tiber delta, central Italy. *Quaternary Science Reviews 243*, 106470, https://doi.org/10.1016/j.quascirev.2020.106470.

Pereira, A., Nomade, S., Falguères, C., Bahain, J.-J., Tombret, O., Garcia, T., Voinchet, P., Bulgarelli, G.-M. & Anzidei, A.-P. 2017: $^{40}Ar/^{39}Ar$ and ESR/U-series data for the La Polledrara di Cecanibbio archaeological site (Lazio, Italy). *Journal of Archaeological Science: Reports 15*, 20–29.

Perini, G., Francalanci, L., Davidson, J. P. & Conticelli, S. 2004: Evolution and genesis of magmas from Vico Volcano, Central Italy: multiple differentiation pathways and variable parental magmas. *Journal of Petrology 45*, 139–182.

Petrosino, P., Jicha, B. R., Mazzeo, F. C., Ciaranfi, N., Girone, A., Maiorano, P. & Marino, M. 2015: The Montalbano Jonico marine succession: an archive for distal tephra layers at the Early–Middle Pleistocene boundary in southern Italy. *Quaternary International 383*, 89–103.

Piva, A., Asioli, A., Schneider, R. R., Trincardi, F., Andersen, N., Colmenero-Hidalgo, E., Dennielou, B., Flores, J. A. & Vigliotti, L. 2008: Climatic cycles as expressed in sediments of the PROMESS1 borehole PRAD1-2, central Adriatic, for the last 370 ka: 1. Integrated stratigraphy. *Geochemistry Geophysics Geosystems 9*, Q01R01, https://doi.org/10.1029/2007GC001713.

R Core Team 2022: *R: A Language and Environment for Statistical Computing.* R Foundation for Statistical Computing, Vienna.

Railsback, L. B., Gibbard, P. L., Head, M. J., Voarintsoa, N. R. G. & Toucanne, S. 2015: An optimized scheme of lettered marine isotope substages for the last 1.0 million years, and the climatostratigraphic nature of isotope stages and substages. *Quaternary Science Reviews 111*, 94–106.

Renne, P. R., Balco, G., Ludwig, K. R., Mundil, R. & Min, K. 2011: Response to the comment by WH Schwarz et al. on "Joint determination of 40 K decay constants and $^{40}Ar/^{40}K$ for the Fish Canyon sanidine standard, and improved accuracy for $^{40}Ar/^{39}Ar$ geochronology" by PR Renne et al. (2010). *Geochimica et Cosmochimica Acta 75*, 5097–5100.

Rolandi, G., Bellucci, F., Heizler, M. T., Belkin, H. E. & De Vivo, B. 2003: Tectonic controls on the genesis of ignimbrites from the Campanian Volcanic Zone, southern Italy. *Mineralogy and Petrology 79*, 3–31.

Ryan, W. B. F., Carbotte, S. M., Coplan, J. O., O'Hara, S., Melkonian, A., Arko, R., Weissel, R. A., Ferrini, V., Goodwillie, A., Nitsche, F., Bonczkowski, J. & Zemsky, R. 2009: Global Multi-Resolution Topography synthesis. *Geochemistry Geophysics Geosystems 10*, 1525–2027.

Sbrana, A., Marianelli, P. & Pasquini, G. 2018: Volcanology of Ischia (Italy). *Journal of Maps 14*, 494–503.

Sottili, G., Arienzo, I., Castorina, F., Gaeta, M., Giaccio, B., Marra, F. & Palladino, D. M. 2019: Time-dependent Sr and Nd isotope variations during the evolution of the ultrapotassic Sabatini Volcanic District (Roman province, Central Italy). *Bulletin of Volcanology 81*, 67, https://doi.org/10.1007/s00445-019-1324-7.

Sottili, G., Palladino, D. M., Marra, F., Jicha, B., Karner, D. B. & Renne, P. 2010: Geochronology of the most recent activity in the Sabatini Volcanic District, Roman Province, central Italy. *Journal of Volcanology and Geothermal Research 196*, 20–30.

Sottili, G., Palladino, D. M. & Zanon, V. 2004: Plinian activity during the early eruptive history of the Sabatini volcanic district, central Italy. *Journal of Volcanology and Geothermal Research 135*, 361–379.

Sulpizio, R., Zanchetta, G., Caron, B., Dellino, P., Mele, D., Giaccio, B., Insinga, D., Paterne, M., Siani, G., Costa, A., Macedonio, G. & Santacroce, R. 2014: Volcanic ash hazard in the Central Mediterranean assessed from geological data. *Bulletin of Volcanology 76*, 866, https://doi.org/10.1007/s00445-014-0866-y.

Vakhrameeva, P., Koutsodendris, A., Wulf, S., Fletcher, W. J., Appelt, O., Knipping, M., Gertisser, R., Trieloff, M. & Pross, J. 2018: The cryptotephra record of the Marine Isotope Stage 12 to 10 interval (460–335 ka) at Tenaghi Philippon, Greece: exploring chronological markers for the Middle Pleistocene of the Mediterranean region. *Quaternary Science Reviews 200*, 313–333.

Vakhrameeva, P., Koutsodendris, A., Wulf, S., Portnyagin, M., Appelt, O., Ludwig, T., Trieloff, M. & Pross, J. 2021: Land-sea correlations in the Eastern Mediterranean region over the past c. 800 kyr based on macro- and cryptotephras from ODP Site 964 (Ionian Basin). *Quaternary Science Reviews 255*, 106811, https://doi.org/10.1016/j.quascirev.2021.106811.

Vakhrameeva, P., Wulf, S., Koutsodendris, A., Tjallingii, R., Fletcher, W. J., Appelt, O., Ludwig, T., Knipping, M., Trieloff, M. & Pross, J. 2019: Eastern Mediterranean volcanism during marine isotope stages 9 to 7e (335–235 ka): insights based on cryptotephra layers at Tenaghi Philippon, Greece. *Journal of Volcanology and Geothermal Research 380*, 31–47.

Wagner, B. and 47 others 2019: Mediterranean winter rainfall in phase with African monsoons during the past 1.36 million years. *Nature 573*, 256–260.

Wagner, B., Tauber, P., Francke, A., Leicher, N., Binnie, S. A., Cvetkoska, A., Jovanovska, E., Just, J., Lacey, J. H., Levkov, Z., Lindhorst, K., Kouli, K., Krastel, S., Panagiotopoulos, K., Ulfers, A., Zaova, D., Donders, T. H., Grazhdani, A., Koutsodendris, A., Leng, M. J., Sadori, L., Scheinert, M., Vogel, H., Wonik, T., Zanchetta, G. & Wilke, T. 2023: The geodynamic and limnological evolution of Balkan Lake Ohrid, possibly the oldest extant lake in Europe. *Boreas 52*, 1–26.

Wulf, S., Keller, J., Paterne, M., Mingram, J., Lauterbach, S., Opitz, S., Sottili, G., Giaccio, B., Albert, P. G., Satow, C., Tomlinson, E. L., Viccaro, M. & Brauer, A. 2012: The 100–133 ka record of Italian explosive volcanism and revised tephrochronology of Lago Grande di Monticchio. *Quaternary Science Reviews 58*, 104–123.

Zanchetta, G., Regattieri, E., Giaccio, B., Wagner, B., Sulpizio, R., Francke, A., Vogel, H., Sadori, L., Masi, A., Sinopoli, G., Lacey, J. H., Leng, M. J. & Leicher, N. 2016: Aligning and synchronization of MIS 5 proxy records from Lake Ohrid (FYROM) with independently dated Mediterranean archives: implications for DEEP core chronology. *Biogeosciences 13*, 2757–2768.

Zanchetta, G., Sulpizio, R., Roberts, N., Cioni, R., Eastwood, W. J., Siani, G., Caron, B., Paterne, M. & Santacroce, R. 2011:

Tephrostratigraphy, chronology and climatic events of the Mediterranean basin during the Holocene: an overview. *Holocene 21*, 33–52.

Supporting Information

Additional Supporting Information to this article is available at http://www.boreas.dk.

Table S1. Analytical details of ^{40}Ar/^{39}Ar measurements.